Menin maintains enhancer-promoter interactions in a leukemia-specific manner

Vassilena Sharlandjieva[1,2], Catherine Chahrour[1], Frederik H. Lassen[3], Joseph C. Hamley[1], Andreas Damianou[2,4], Nicholas Denny[1], Alastair L. Smith[1], Svenja S. Hester[2], Iolanda Vendrell[2], Ronald W. Stam[5], Marina Konopleva[6], Anindita Roy[1,7] James O. J. Davies[1], Nicholas T. Crump[8], Benedikt M. Kessler[2,4*] and Thomas A. Milne[1*]

[1] MRC Molecular Haematology Unit, MRC Weatherall Institute of Molecular Medicine, Radcliffe Department of Medicine, University of Oxford, Oxford OX3 9DS, UK.

[2] Target Discovery Institute, Centre for Medicines Discovery, Nuffield Department of Medicine, University of Oxford, Roosevelt Drive, OX3 7FZ Oxford, UK

[3] Big Data Institute, Nuffield Department of Medicine, University of Oxford, Oxford, UK

[4] Chinese Academy of Medical Sciences Oxford Institute, Nuffield Department of Medicine, University of Oxford, Roosevelt Drive, OX3 7BN Oxford, UK

[5] Princess Máxima Center for Pediatric Oncology, Heidelberglaan 25, 3584, Utrecht, The Netherlands

[6] Montefiore Einstein Cancer Center, Department of Oncology and Cell Biology, 1300 Morris Park Avenue, Bronx, NY 10461, USA.

[7] Department of Paediatrics, University of Oxford, Oxford OX3 9DU, UK.

[8] Hugh and Josseline Langmuir Centre for Myeloma Research, Centre for Haematology, Department of Immunology and Inflammation, Imperial College London, London W12 0NN, UK

*These authors jointly supervised this work.

Correspondence: benedikt.kessler@ndm.ox.ac.uk (B.M.K); thomas.milne@imm.ox.ac.uk (T.A.M.)

Short title: Menin regulates enhancers in MLL::AF4 leukemia

Disclosures: T.A.M. is a paid consultant for Dark Blue Therapeutics Ltd. (now Amgen). F.H.L is a director and shareholder at Omos Biosciences Ltd. J.O.J.D is a founder of and consultant for Nucleome Therapeutics.

Funding: This work was funded by the Wellcome Trust and Medical Research Council (MRC, UK) Molecular Haematology Unit grant MC_UU_00029/6. Patient samples and data used in this study were provided by VIVO Biobank, supported by Cancer Research UK & Blood Cancer UK (Grant no. CRCPSC-Dec21\100003), or by the INTERFANT studies.

Abstract

Inhibition of the protein-protein interaction between Mixed Lineage Leukemia (MLL) and Menin is a promising therapy for both high-risk *MLL*-rearranged and *NPM1*-mutant (NPM1c) acute leukemias, yet the mechanistic basis of this dependency in distinct contexts remains unclear. By comparing the transcriptional responses of MLL::AF4 and NPM1c leukemia models to Menin inhibition, we find broad, acute transcriptional dysregulation in MLL::AF4 cells, but minor transcriptional consequences in NPM1c cells, despite similarities in Menin promoter occupancy. Using high-resolution Micro-Capture-C, we discover that Menin drives enhancer activity and maintains enhancer-promoter contacts in MLL::AF4 cells but not in NPM1c cells. Crucially, Menin is also essential for patient-specific enhancer function in primary MLL::AF4 leukemia samples. Proteomic analysis further demonstrates that Menin associates with distinct transcriptional and elongation complexes in MLL::AF4 compared to NPM1c cells, supporting a context-dependent mechanism of action. Together, these findings establish that Menin is not a uniform transcriptional cofactor, but a context-dependent regulator of enhancer connectivity, and identifies enhancer-promoter architecture as a selective vulnerability in MLL-rearranged leukemia.

Introduction

Chromatin is the DNA/protein complex in the cell that influences both transcriptional activity and cell identity.[1] In leukemia, frequent mutations in chromatin-modifying proteins and transcription factors trigger oncogenic transcription, often hijacking endogenous machinery, which leads to the expansion of immature progenitor cells.[2,3] As a result, epigenetic enzymes, including transcriptional repressors (EZH2, HDAC, LSD1) and activators (P300, bromodomain proteins, DOT1L),[4–6] have become promising targets in hematological malignancies.

Menin is a chromatin protein that has emerged as a key vulnerability in high-risk leukemia. Menin is a component of multiple complexes,[7–10] but its best studied role is as a member of the Mixed Lineage Leukemia complex (MLL1 or MLL, also known as KMT2A), where it interacts directly with the N-terminus of MLL. Rearrangements of the *MLL* gene (*MLL*r) give rise to oncogenic fusion proteins sufficient to drive leukemia, and account for approximately 10% of acute leukemias overall but up to 90% of infant B acute lymphoblastic leukemia (ALL).[11–13] Patients with *MLL* rearrangements have a worse prognosis and a poor response to conventional chemotherapy,[14] highlighting an unmet clinical need. MLL fusion proteins (MLL-FPs), most commonly MLL::AF4 in infants and MLL-AF9 in adults,[15] assemble a large protein complex, including Menin, which activates gene expression through both epigenetic and transcription elongation mechanisms.[16–18] Menin is essential for leukemia initiation in the presence of MLL-FPs, facilitating oncogenic transcription by stabilizing MLL-FPs at hematopoietic genes, such as *MEIS1.*[19]

Menin inhibitors disrupt the Menin-MLL/MLL-FP interaction and initially aimed to target *MLL*r leukemia.[20] However, they have also been found to be effective in acute myeloid leukemia (AML) with *NPM1* mutations.[21–25] Affecting 30% of patients, *NPM1* mutations are the most common genetic lesion in AML,[26] meaning that Menin inhibition (MENi) has the potential to benefit a large group of patients. *NPM1* mutations are commonly frameshifts in the C-terminus that disrupt a nucleolar localisation signal.[27–30] They have a dual effect on the typically nucleolar nucleophosmin protein—a portion of the mutant protein ("NPM1c") aberrantly localizes to the cytoplasm, while a small proportion in the nucleus can function as a transcription activator by directly binding at a subset of Menin-MLL target genes.[21,24] NPM1c is associated with expression of the *HOXA/B* cluster and their co-factor *MEIS1*—similar to MLLr leukemias.[31,32]

Menin inhibitors cause the loss of Menin binding at chromatin and downregulation of key MLL-FP and NPM1c targets.[22,33] However, as Menin is part of distinct complexes in *MLLr* and NPM1c leukemias, it is unclear if Menin has direct role in driving transcription in these distinct

leukemia subtypes. Both MLL-FPs and NPM1c are transcriptional activators, binding at active promoters and spreading into gene bodies.[24,34] In addition to promoters, MLL-FPs have also been shown to bind enhancers[35–37]—non-coding regulatory elements that modulate gene transcription from a distance.[38] The resulting aberrant enhancer activation is a key mechanism driving oncogenic gene expression programmes in *MLL*r leukemia.[36,39,40] While this implicates Menin in the maintenance of enhancer activity in the presence of MLL-FPs, Menin also binds a subset of enhancers in ER+ breast cancer cells with wildtype *MLL*—suggesting a possible role for Menin in driving enhancer function more generally.[41] NPM1c binding outside promoters has also been reported,[24] but whether it is functionally maintaining enhancer activity—and whether it requires Menin for this—remains unknown. Better understanding the role of Menin in transcription in different contexts could inform our interpretation of patient response, relapse and resistance in ongoing clinical trials (summarized in[42] and[43]).

In this paper, we show that MENi triggers large scale, acute transcriptional dysregulation in MLL::AF4 ALL cells but not in NPM1c AML cells. This difference is associated with Menin binding at intragenic enhancers in the presence of MLL::AF4, where it facilitates enhancer-promoter contacts at key oncogenes—an activity absent in NPM1c cells. We also show a greater enrichment of transcription regulators and elongation factors in the Menin interactome in MLL::AF4 cells compared to NPM1c cells, suggesting a more central role for Menin in gene activation. Together, our characterization of Menin activity in distinct leukemia subtypes demonstrates that the mechanism by which MENi disrupts oncogenic transcription is unique to context-specific Menin function.

Results

Menin inhibition has distinct transcriptional effects in MLL::AF4 and NPM1c cells

While current models for the therapeutic function of MENi state that destabilized MLL-FP or NPM1c binding trigger decreased gene expression,[44] most studies of the effects of MENi report transcriptional changes after multi-day treatments and so early, direct effects on Menin-bound genes in different contexts are unclear.[25,33] We sought to compare the effects of MENi on nascent transcription at an early timepoint, using SEM and OCI-AML3 cells as models of MLL::AF4 ALL and NPM1c AML respectively. As a reference to a model of insensitivity to MENi, we used RCH-ACV cells, an E2A-PBX1-driven ALL cell line. Following treatment with the Menin inhibitor VTP50469 (250 nM) for 24 hours, Menin binding was depleted from transcription start sites (TSS) genome-wide in each cell line (Figure S1A), regardless of inhibitor sensitivity status. Transient Transcriptome RNA-seq (TT-seq) at this timepoint revealed extensive transcriptional changes in SEM (MLL::AF4) cells, and surprisingly few changes in OCI-AML3 (NPM1c) cells (Figure 1A). MENi resulted in 1874 differentially expressed genes in SEM cells, the majority (1058) of which were downregulated. They included MLL::AF4 targets such as *FLT3, MEF2C* and *JMJD1C,*[33] but not *HOXA9* or *MEIS1*. In contrast, OCI-AML3 (NPM1c) cells had 103 differentially expressed genes of which 72 were downregulated—including *MEIS1*, which is considered the critical Menin-dependent vulnerability in these cells.[21,23,25]

This contrast in transcriptional consequences following MENi was correlated with effects on cell fitness at 48 h MENi. Using CellTiterGlo assays, we observed that SEM cells were highly sensitive, with an IC50 of 45.5 nM, whereas OCI-AML3 cells did not reach IC50 even at the highest concentration of inhibitor (62.5 μM) tested, similar to the insensitive RCH-ACV cells. (Figure S1B). In contrast, colony formation assays over a two-week period showed that both SEM and OCI-AML3 colony formation was inhibited completely with MENi (Figure S1C).

To understand why Menin loss has broad and immediate transcriptional consequences in SEM (MLL::AF4) cells yet highly restricted effects in OCI-AML3 (NPM1c) cells, we compared Menin occupancy at the promoters of differentially expressed genes in each cell line. Curiously, we found a significant association between Menin promoter binding and gene downregulation in SEM (p = 1.52e-45, chi-square test) but not in OCI-AML3 (p = 0.13) (Figure S1D). Downregulated genes in SEM cells also had higher average Menin enrichment compared to upregulated or unchanged genes (Figure S1E). Yet, when we intersected Menin-bound promoters in the two cell lines, we found that the majority (6,091) were shared between cell

152 lines (Figure 1B, left), while down-regulated Menin targets were predominantly unique to SEM
153 cells (Figure 1C, right). This indicated that common Menin occupancy at promoters was not
154 predictive of transcriptional sensitivity to MENi in SEM and OCI-AML3 cells.
155
156 Menin is thought to stabilize MLL::AF4 and NPM1c chromatin binding and both these
157 oncoproteins have been shown to activate genes by recruiting RNA polymerase II and
158 transcription elongation factors.[24,45,46] Previous work has identified 2,597 unique genes bound
159 by MLL::AF4 in SEM cells,[34] whereas only 44 genes are NPM1c-bound in OCI-AML3 cells.[21]
160 It is therefore possible that the context-dependent regulation of genes by these oncoproteins
161 determines the scale of transcription dysregulation in response to MENi. However, MENi
162 disrupts MLL::AF4 binding at only a subset of its target promoters,[33] and indeed we also saw
163 that after 24 h MENi, only 16.1% (176/1058) of downregulated genes in SEM cells had a
164 concordant decrease in MLL::AF4 promoter occupancy (Figure S1F, G). Similarly, 8/72 down-
165 regulated genes in OCI-AML3 cells had decreased NPM1c binding. Taken together, our data
166 indicated that neither high Menin occupancy at promoters nor loss of MLL::AF4 binding can
167 fully explain the large number of dysregulated genes in SEM (MLL::AF4) cells following MENi.
168
169 **Menin binds enhancer elements**
170
171 To further investigate why Menin has a more dramatic and immediate effect on transcription
172 in SEM cells and not OCI-AML3 cells, we probed for the presence of Menin binding outside of
173 gene promoters. We annotated Menin ChIP-seq peaks to promoters, intragenic enhancers
174 and intergenic enhancers, and linked them to genes using the nearest TSS. This confirmed
175 Menin binding at a subset of enhancers in both SEM and OCI-AML3 cells, although less
176 frequently than its known enrichment at promoters (Figure 1C). For example, we saw Menin-
177 bound domains overlapping with H3K27ac in the gene bodies of *ARID1B*, *CDK6*, and *PAN3,*
178 all of which were larger in SEM (MLL::AF4) cells relative to OCI-AML3 cells (NPM1c) (Figure
179 1D). Using publicly available AutoCUT&Tag[47] and ChIP-seq data, we also confirmed Menin
180 enrichment outside promoters in additional *MLL*r cell lines (Figure S2A, B), as well as Menin
181 binding at intragenic enhancers in primary patient cells which we profiled using small cell
182 number ChIPmentation[48] (Figure S2C) — indicating that this phenomenon extends beyond the
183 SEM cell model.
184
185 We found that Menin-bound intragenic enhancers were specifically enriched in the proximity
186 of downregulated genes in SEM cells but not OCI-AML3 cells (Figure 1E). This link was
187 stronger for intragenic enhancers compared to intergenic enhancers (Figure S2D); we also
188 identified more total genes linked to Menin-bound intragenic enhancers (807, 55% of genes

189 with an intragenic enhancer) versus intergenic enhancers (220, 35% of genes with an
190 intergenic enhancer) in SEM cells. This observation was in line with previous work showing
191 that Menin can spread into gene bodies in the presence of MLL::AF4.[34] Intragenic Menin-
192 bound enhancers linked to downregulated genes had higher levels of Menin and
193 MLL/MLL::AF4 in SEM cells, and to a lesser extent in OCI-AML3 cells (Figure 1F). Upon MENi,
194 intragenic enhancers had reduced MLL::AF4 / MLL binding and, more subtly, H3K27ac. A
195 similar effect was observed at Menin-bound intergenic enhancers (FigureS4D). Given the
196 unique enrichment of Menin-bound putative intragenic enhancers in SEM cells, we sought to
197 further characterise the effects of Menin inhibition on enhancer activity our cell line models.
198
199 **Menin regulates enhancer activity in MLL::AF4 cells**
200
201 A key attribute of enhancers is physical proximity with their target promoters in the 3D
202 organisation of the genome.[49–51] As a result, annotating enhancers to the nearest TSS may
203 not reveal the true target promoter; instead, high-resolution Chromatin Confirmation Capture
204 techniques are needed to link enhancers and promoters. We have previously shown using
205 Capture-C that enhancers occupied by the MLL::AF4 complex lose promoter contact upon
206 knock-down or enzymatic inhibition of complex components.[36,37] To test whether Menin
207 binding also maintains enhancer-promoter contacts, we used the higher-resolution Micro-
208 Capture-C (MCC)[52] to identify enhancer contacts for key gene promoters in SEM and OCI-
209 AML3 cells (Figure 2A). Our panel of promoter viewpoints included key MLL::AF4 and NPM1c
210 targets, genes sensitive to MENi, and genes linked to Menin-bound enhancers using nearest
211 TSS annotation in both cell lines (Supplementary File 1, Figure S3A).
212
213 We filtered MCC peaks — representing regions in contact with the sampled gene promoters
214 — to those overlapping with H3K27ac to define putative functional promoter interactions.
215 Menin was enriched at 69% of promoter interactions for 43 genes analysed in SEM (MLL::AF4)
216 cells, but only 7.5% of interaction sites for 42 genes analysed in OCI-AML3 (NPM1c) cells
217 (Figure 2B). The majority (46%) of Menin-bound enhancers in SEM cells were within introns,
218 followed by MCC peaks (contacts) in other promoters (37%). In contrast, Menin was primarily
219 enriched in other promoter regions (57%) in contact with the OCI-AML3 promoter viewpoints.
220 This contrast emphasized that Menin function is primarily restricted to key promoters in OCI-
221 AML3 cells, whereas intragenic spreading[34] in SEM cells can be linked to enhancer activity.
222
223 Clustering promoter contact sites (MCC peaks) based on chromatin features revealed that
224 Menin-bound enhancer-promoter contacts also had higher MLL/MLL::AF4 and H3K27ac in
225 both cell lines, as well as NPM1c enrichment OCI-AML3 (Figure S3B). Upon MENi for 24

226 hours, enhancers with the highest levels of Menin (cluster 1, Figure S3B) also lost MLL::AF4
227 binding and H3K27ac in SEM cells. In contrast, in OCI-AML3 cells, H3K27ac and NPM1c
228 remained unaffected at the Menin-enriched contacts, suggesting a unique sensitivity to MENi
229 in SEM cells.
230
231 We next asked whether MENi for 24 hours affected the ability of enhancer loci to interact with
232 target promoters. To quantify changes in enhancer-promoter interactions upon MENi across
233 all the sampled viewpoints, we calculated the change in the mean count of unique ligation
234 junctions at each interaction site. In SEM cells, 49 interaction sites had a significant change in
235 interaction frequency (Mann Whitney U test, FDR q-value < 0.05); of the decreased
236 interactions, 90% (39/43) overlapped with Menin binding (Figure 2C). The decrease in
237 promoter interactions with Menin-bound enhancers was significantly lower than sites lacking
238 Menin binding (Wilcoxon test *p*-value < 0.01), pointing to a specific Menin inhibitor-driven
239 effect. Conversely, there were no significant changes in interactions in OCI-AML3 cells,
240 including at Menin-bound sites, suggesting that Menin is dispensable for enhancer-promoter
241 contacts in these cells.
242
243 The *RUNX1* locus illustrated the differential effects of MENi on enhancer activity (Figure 2D).
244 In both SEM and OCI-AML3 cells, the major transcript isoform of *RUNX1* initiates at intron 3
245 (Figure S3C), so we used this site for the MCC capture enrichment. This region contacts the
246 *RUNX1* promoter and several regions in intron 2 (Figure 2C, top, yellow highlights). In SEM
247 cells, Menin inhibition leads to a decrease in interaction frequency with enhancers in intron 2,
248 which we did not observe in OCI-AML3 cells. Sites of decreased interaction had higher Menin
249 enrichment in SEM cells, indicating an SEM-specific Menin-bound enhancer cluster (Figure
250 2C, bottom, yellow highlights). The collapse of the intragenic Menin-bound enhancers in SEM
251 cells correlates with decreased *RUNX1* expression following MENi (Figure 2C, bottom),
252 whereas expression was unaffected in OCI-AML3 cells.
253
254 In OCI-AML3 cells, the NPM1c target gene *BAHCC1* has three Menin-bound enhancer regions
255 (Figure 2E). At two of them, we observed a decreased interaction frequency on average (log2
256 fold change < 0), but this was not statistically significant (FDR > 0.05). H3K27ac, NPM1c
257 binding, and gene expression were also unaffected despite Menin loss (Figure 2E, Figure
258 S3D). This suggests that while Menin may support enhancer-promoter contacts to a more
259 limited extent at select genes, gene transcription is less dependent on Menin in such cases.
260 The intragenic Menin-bound enhancers observed in *ARID1B*, *CDK6* and *PAN3* (Figure 1D)
261 also had more dramatically reduced contacts with the promoter in SEM cells (Figure S3E).
262

263 **Collapse of intragenic-bound enhancers downregulates key genes**
264
265 To further characterize Menin-bound enhancers and their impact on gene regulation in SEM
266 (MLL::AF4) cells, we focused on decreased Menin-bound contacts. The majority (61%) of
267 these were within introns or other promoters (Figure 3B), and were also enriched for Menin
268 binding in infant ALL patient samples with MLL::AF4, but not in OCI-AML3 cells or our adult
269 NPM1c patient sample (Figure S4A).
270
271 Given that MENi led to both decreased H3K27ac and MLL::AF4 at MCC peaks with high levels
272 of Menin binding in SEM cells (Figure S3B), we sought to examine the relationship between
273 these factors and interaction frequency. At decreased interaction sites (Figure 3B, cyan data
274 points), the loss of interaction frequency correlated more with reduced MLL::AF4 enrichment—
275 although this correlation was still weak (R^2 = 0.32). Prior to inhibition, decreased interaction
276 sites had higher Menin enrichment relative to unchanged peaks (Figure S4B), suggesting that
277 these sites may be more sensitive to Menin levels to stabilise MLL::AF4 and contacts with the
278 promoter.
279
280 To confirm that Menin-bound enhancer-promoter contacts were functionally associated with
281 transcription, we linked the most significant interaction change to gene expression and
282 observed that downregulated genes were more likely to have a decreased enhancer-promoter
283 contact in SEM cells (Figure 3C). Among the genes with a concordant decrease in enhancer
284 contacts and expression were *ARID1B, FLT3, PROM1*, and *CDK6* (Figure 3D)—key
285 oncogenes at which the MLL::AF4 complex has previously been shown to sustain enhancer-
286 promoter contacts[36,37,] confirming that enhancer activation and maintenance of proximity is an
287 important function of Menin in MLL::AF4 leukemia.
288
289 **Menin maintains patient-unique enhancer elements in infant MLL::AF4 patient cells**
290
291 We recently showed that enhancer activity can drive transcriptional heterogeneity in ALL
292 patient cells that all carry the MLL::AF4 fusion.[39] The largest proportion of enhancers that
293 varied between patients were also found within intronic elements. While a machine learning
294 prediction model identified the MLL::AF4 fusion and the PAF1 complex as the main predictive
295 features of heterogenous enhancer activity, without flagging Menin as an important feature,
296 we nonetheless hypothesized that Menin inhibition may be effective in disrupting patient-
297 unique enhancers. To test this, we performed ChIPmentation and MCC in three primary infant
298 ALL samples with MLL::AF4 fusions following Menin inhibition (Figure 4A, Figure S5A).
299

300 First, we confirmed that Menin was enriched at a subset of MCC peaks (Figure 4B), although
301 this was a lower proportion than we observed in SEM cells (Figure 3B). Given heterogeneity
302 in Menin binding and enhancer activity among patients, we focused on comparing the effects
303 of MENi on enhancers within each patient individually, rather than treating the patients as
304 biological replicates and applying strict statistical thresholds (see Methods for additional
305 details). We observed decreased (LFC < 0) interactions at some Menin-bound enhancer
306 domains, with the largest changes in interactions tending to occur at sites with the greatest
307 Menin enrichment at the enhancer (Figure 4C). Most of the reduced contacts mapped to other
308 promoters (within 2 Kb of a TSS), followed by reduced enhancers within introns and exons
309 (Figure 4D).
310
311 Although each patient carried an MLL::AF4 fusion, we observed heterogeneity in Menin
312 binding and consequently in enhancer usage. For example, Patient 1823 (P1823) exhibited a
313 unique Menin-bound enhancer at an intergenic site between the *ANTXR2* and *PRDM8* loci
314 (Figure 4E, top, yellow highlight). Interestingly, the *ANTXR2* promoter contacts this region in
315 all 3 patients, but the *PRDM8* promoter interacts with it exclusively in P1823. Menin inhibition
316 specifically reduced the interaction with the *PRDM8* promoter in this patient sample (Figure
317 4E, bottom, yellow highlights) following loss of Menin binding (Figure S5B).
318
319 The *ARID1B* locus represented another region of variation for enhancer activity and Menin
320 binding in the patients. P873 exhibited a uniquely large Menin-bound enhancer in intron 4
321 (Figure 4F, left, box 2), whereas in P9422, Menin occupied an intergenic enhancer upstream
322 of the *ARID1B* promoter (Figure 4F, left, box 1). Following Menin inhibition, the P873 *ARID1B*
323 promoter specifically lost interactions with the intron 4 Menin-bound site, whereas the P9422
324 *ARID1B* promoter lost interactions with its upstream Menin-bound enhancer, which correlated
325 with reduced Menin occupancy (Figure S5C). Together, these observations suggest that
326 Menin inhibition can disrupt enhancer-promoter contacts even in heterogeneous patient cells
327 harboring MLL::AF4.
328
329 **Menin interactors point to its context-specific roles in transcription**
330
331 We have previously shown that MLL::AF4 and interacting complexes such as DOT1L, FACT
332 and PAF1—which are traditionally associated with transcription elongation[53–55]—can also
333 regulate enhancer activity in SEM cells[36,37]. Consequently, we sought to interrogate whether
334 Menin interacts with distinct protein complexes, such as additional co-activators in the
335 presence of MLL::AF4, to facilitate distinct transcriptional processes based on the leukemia
336 context.

337
338 To test this, we returned to the cell line models to perform endogenous Menin co-
339 immunoprecipitation from nuclear extracts followed by mass spectrometry (IP-MS) in SEM
340 (MLL::AF4) and OCI-AML3 (NPM1c) cells (Figure 5A). Protein abundances in the nuclear
341 proteomes and immunoprecipitates were highly correlated (Pearson $r \geq 0.7$) between SEM
342 and OCI-AML3 cells (Figure S6A). We defined Menin interactors as proteins statistically
343 enriched (FDR < 0.01) over IgG controls and compared this set between SEM and OCI-
344 AML3 cells (Figure 5B). Among the most differentially enriched proteins were lineage-
345 specific factors such as PAX5 in SEM cells and MNDA in OCI-AML3 cells. Interestingly, we
346 also found that the acetyltransferase P300, which regulates promoter and enhancer activity
347 via H3K27ac[56,57], was also more enriched in the Menin interactome in SEM cells compared
348 to OCI-AML3. As such, we hypothesised that MLL::AF4 may also co-opt Menin for driving
349 enhancer activation in co-operation with a unique interactome of more general transcriptional
350 co-activators.
351
352 To identify general transcription complexes associated with Menin, we performed an
353 enrichment analysis for protein complexes in the Corum database[58] for each cell line. As
354 expected, we found the MLL1 complex enriched in both SEM and OCI-AML3 cells (Figure
355 5C). However, members of FACT, SAGA, and MSH2/6 DNA repair machinery were
356 specifically enriched in SEM cells. The expression of these complex components was highly
357 correlated in the nuclei of both SEM and OCI-AML3 cells (Figure S6B), indicating that the
358 observed differential enrichment reflects interactions with Menin rather than simply differential
359 expression between these cell lines.
360
361 To assess whether the transcription-associated complexes uniquely enriched in SEM cells are
362 also key for cell survival, we referenced DepMap gene effect scores for the genes making up
363 these complexes. Gene effect scores, where a score of -1 represents the median of common
364 essential genes[59], were highly correlated in SEM and OCI-AML3 cells, with a subset emerging
365 as essential in both cell lines (Figure S6C). The selective enrichment of these transcriptional
366 activators in the SEM Menin interactome may explain the rapid transcriptional changes and
367 associated short-term sensitivity to Menin inhibition, as Menin may be repurposed to stabilise
368 the co-operation of these complexes with the MLL::AF4 complex. Menin inhibition for 24 h
369 indeed led to decreased (LFC < 0) enrichment of some transcriptional complex components
370 in Menin immunoprecipitations (Figure 5D), suggesting that additional factors may rely on
371 Menin binding to chromatin to maintain their association with the MLL::AF4 complex.
372
373

374 **Distinct roles for Menin in MLL::AF4 and NPM1-mutant leukemia**

375

376 Together, our data point to distinct Menin activity in MLL::AF4 and NPM1c acute leukemias in
377 transcriptional activation and modulating enhancer activity (Figure 5E). In MLL::AF4 cells,
378 Menin functions as a transcriptional co-activator, facilitating promoter–enhancer contacts and
379 interacting with additional transcription activators. Menin inhibition therefore results in rapid,
380 widespread changes in transcription in MLL::AF4 cells In contrast, in NPM1c AML cells, Menin
381 loss has a restricted acute effect on transcription at small subset of target loci, likely due to a
382 more indirect effect on stabilizing NPM1c binding rather than directly interacting with
383 transcription elongation complexes. These differences in Menin protein complex composition
384 and Menin activity at enhancers could explain the greater transcriptional disruption observed
385 with MENi in MLL::AF4 compared to NPM1c cells.

386

387 **Discussion**

388

389 Menin inhibition is a promising targeted therapy for high-risk *MLL*-rearranged and *NPM1*-
390 mutant acute leukemias, which both depend on Menin for the expression of key genes and
391 cell survival. However, our data highlight that the mechanism by which Menin affects aberrant
392 transcription differs between the two diseases. Upon MENi, SEM cells (MLL::AF4) exhibited
393 rapid transcriptional dysregulation, which affected thousands of genes, and loss of intragenic
394 Menin-bound enhancer activity. Menin-bound enhancers were similarly affected in primary
395 patient cells with MLL::AF4, despite enhancer heterogeneity. On the other hand, OCI-AML3
396 cells (NPM1c) showed transcription changes in approximately one hundred genes at the same
397 timepoint while enhancer activity was unaffected. Therefore, the major contribution of Menin
398 to transcription is highly context-dependent, and linked to its enhancer activity and the protein
399 complexes it participates in.

400

401 Our Menin co-immunoprecipitations from SEM and OCI-AML3 cells revealed that Menin
402 interacts with transcription regulators with some cell-type specificity. This adds to a complex
403 body of literature illuminating context-specific Menin interactions that can trigger either
404 transcription activation or repression[9]. Focusing on transcription regulators, we found that
405 P300 and the FACT complex were more enriched in the Menin interactome of SEM cells
406 compared to OCI-AML3 cells. Given that loss of either PAF1, FACT [36] or H3K79me2/3[37] can
407 lead to decreased enhancer promoter interactions at MLL::AF4-bound enhancers, these
408 multiple vulnerabilities suggest that the overall stability of the MLL::AF4 complex, rather than
409 one specific component, may be key to the maintenance of enhancer-promoter contacts and
410 transcription. This points to a possible role for Menin in stabilizing these factors at enhancers
411 in MLL::AF4 ALL cells.

412

413 Both MLL-FPs and NPM1c are transcriptional activators that require Menin binding at a subset
414 of their target promoters. Wang *et. al.* (2023) showed that chromatin-associated NPM1c forms
415 transcriptional hubs, which include elongation factor ENL, Menin, and RNA Polymerase II,
416 through multivalent interactions[24]. However, they also showed that NPM1c did not alter
417 chromatin or trigger new transcription when introduced de novo; rather it further upregulates
418 genes with an established baseline expression. MLL-FPs on the other hand, in addition to
419 maintaining expression of active genes via the recruitment of co-activators and elongation
420 factors[45,46], can also activate self-renewal genes characteristic of hematopoietic stem cells
421 when exogenously expressed[60]. Recently, it was demonstrated that MLL-AF10 can activate
422 new enhancer elements[40]. Therefore, destabilizing MLL::AF4—a more potent and wide-
423 spread transcriptional activator compared to NPM1c—via MENi could be more disruptive to

424 the oncogenic gene expression programme, indicating that that Menin is co-opted as a
425 transcriptional activator to a greater extent than when in a complex with NPM1c.
426
427 While our analysis focused on MLL::AF4 ALL, it has also previously been observed that
428 leukemia cell identity can dictate the response to MENi. Comparing 4-day treatments with
429 Revumenib, a Menin inhibitor used in the clinic, in *MLL*r AML and ALL cells has revealed that
430 MENi rapidly induces apoptosis and cell cycle arrest in *MLL*r-ALL cells, whereas in *MLL*r-AML
431 cells the response is slower and involves differentiation rather than cell death[61]. Therefore,
432 understanding Menin activity in the presence of both different driver mutations and in different
433 leukemia subtypes is key to extending MENi as a therapeutic option to the right patient
434 populations[62]. Following evidence that Menin can regulate the transcriptional activity of NUP98
435 fusion proteins[63] and oncoproteins arising from *UBTF* tandem duplications[64], patients with
436 these lesions are now included in Menin inhibitor clinical trials (e.g. NCT05326516,
437 NCT05360160, NCT04811560, NCT06177067, APAL2020K ITCC-101/COG/PEDAL).
438 Unexpectedly, Menin and its interacting complexes are also an emerging vulnerability in solid
439 tumors[65,66]. How Menin regulates genes in cancers with other driver mutations, and whether
440 its function goes beyond supporting the binding of other oncoproteins on chromatin, remains
441 to be elucidated.
442
443 Monitoring the transcriptional responses to MENi over time could also be key to classifying
444 patient responses as we ascertain resistance mechanisms. The AUGMENT-101 clinical trial
445 reported that mutations in the Revumenib binding pocket on Menin can restore Menin/MLL-
446 FP binding and expression of MLL-FP target genes[67]. However, when resistance arose without
447 new mutations, the leukemias persisted despite the expected downregulation of Menin
448 targets. This suggests that some leukemias can cease to depend on the Menin/MLL-FP
449 transcriptional program despite an initial and sustained response to MENi. Distinct
450 transcriptional responses to MENi, and how they link to clinical outcomes, can therefore
451 provide a rationale for subtype-specific combination therapies.
452

Acknowledgements

We thank Jerry McGeehan (Syndax Pharmaceuticals) for supplying the VTP50469 used in these experiments. V.S. was funded by the Wellcome Trust. A.D. and B.M.K. were supported by the Chinese Academy of Medical Sciences (CAMS) Innovation Fund for Medical Sciences (CIFMS), China (grant number: 2024-I2M-2-001-1). T.A.M. was supported by Medical Research Council (MRC, UK) Molecular Haematology Unit grant MC_UU_00029/6. The work was also supported by Blood Cancer UK grant 24016. N.T.C. was supported by a Kay Kendall Leukemia Fund Intermediate Fellowship (KKL1443). A.R. is supported by a Wellcome Trust Clinical Research Career Development Fellowship (216632/Z/19/Z) and Medical Research Council (MRC, UK) Molecular Haematology Unit grant MC_UU_00029/7. Samples and data used in this study were provided by VIVO Biobank, supported by Cancer Research UK & Blood Cancer UK (Grant no. CRCPSC-Dec21\100003). Scientific illustrations were adapted from Bioicons.com under creative commons licence CC-BY.

Author Contributions

T.A.M, N.T.C., B.M.K., and V.S. conceived the experimental design. V.S., A.D., S.S.H., and A.L.S. carried out experiments. V.S, C.C., F.H.L., and J.C.H. analyzed and curated the data. V.S., C.C, N.T.C., and T.A.M. interpreted the data and wrote the manuscript. N.D. contributed toward MCC experimental design. I.V and S.S.H. developed mass spectrometry methods. R.W.S., M.K., and A.R. provided primary patient material. B.M.K. and T.A.M., provided funding and supervision. All authors reviewed the manuscript.

Data Availability

Genomics data have been deposited in the Gene Expression Omnibus (GEO) as a series under the accession number GSE312345. Mass spectrometry data have been deposited to the ProteomeXchange Consortium via the PRIDE partner repository with the dataset identifier PXD071336. Publicly available cell line data and previously deposited patient data are available in GEO under accession codes: GSM5114291; GSM5139719; GSM5139645; GSM5139689; GSM8657204; GSM8657208; GSM8657184; GSM8657191; GSM5858383; GSM3635683.

Competing Interests

T.A.M. is a paid consultant for and shareholder in Dark Blue Therapeutics Ltd (now Amgen). F.H.L is a director and shareholder at Omos Biosciences Ltd. J.O.J.D is a founder of and consultant for Nucleome Therapeutics. The remaining authors declare no competing interests.

489 **Methods**

490 **Cell culture**

491 SEM cells (DSMZ) were grown in IMDM supplemented with 10% FBS and 1X GlutaMax
492 (Gibco). RCH-ACV and OCI-AML3 cells were grown in RPMI supplemented with 10% FBS
493 and 1X GlutaMax (Gibco). Patient cells were cultured in RPMI supplemented with 5 mg/ml
494 insulin, 5mg/ml transferrin, 5 ng/ml sodium selenite (ITS, Gibco), 200 µg/ml gentamycin, and
495 20% FBS.

496

497 **Patient samples**

498 Infant (aged <1 year at diagnosis) ALL samples iALL28349 and iALL863388 were obtained
499 from Blood Cancer UK Childhood Leukaemia Cell Bank (now VIVO Biobank, United
500 Kingdom) under their ethics approval (REC: 23/EM/0130) and from Our Lady's Children's
501 Hospital, Crumlin, Ireland (REC: 21/LO/0195). The adult AML sample was obtained from MD
502 Anderson Centre, USA, under RB protocol LAB-01-473. Primary *MLL*-rearranged infant ALL
503 patient specimens P1823, P873 and P9422 were collected as part of the INTERFANT
504 studies[68]. Informed consent was obtained from parents or legal guardians to use excess
505 diagnostic material for research purposes, as approved by the institutional review board.
506 These studies were conducted in accordance with the Declaration of Helsinki. All samples
507 were processed and cultured as previously described[69]. Samples were obtained at diagnosis
508 and contained >90% blasts.

509

510 **CellTiterGlo**

511 Cells were treated with a dilution series of VTP50469 fumarate (Syndax Pharmaceuticals) in
512 triplicate wells in an opaque 96 well plate. After 48 h, CellTiterGlo 2.0 reagent (Promega
513 G9241) was added to each well in equal volume to the media. The plate was shaken for 2 min
514 and incubated for 5 min at room temperature, after which luminescence was recorded on a
515 BMG FLUOstar OPTIMA plate reader. The luminescence signal was normalised to DMSO-
516 treated cells and averaged across replicates. The dose response curves were fitted using the
517 R package drc[70].

518

519 **Colony Assay**

520 In duplicate, cells were treated with either 50 nM or 250 nM VTP50469, or DMSO, for 90 min,
521 then added to MethoCult (StemCell Technologies H4100) containing 50 nM or 250 nM
522 VTP50469 or DMSO. Methocult cultures were aliquoted into three replicate 3 cm dishes, for a
523 total of 5 replicate plates per condition. After 10-14 days, the number of colonies was counted
524 under a light microscope and the counts across replicates were averaged.

525

526 **Chromatin Immunoprecipitation followed by Sequencing (ChIP-seq)**
527 For Menin, NPM1c and MLL-N ChIP, cells were fixed for 30 min with 2 mM Di(N-succinimidyl)
528 glutarate (DSG) followed by 30 minutes with 1% formaldehyde. For histone modifications, cells
529 were fixed for 10 minutes with 1% formaldehyde. Fixed cells were lysed in SDS lysis buffer
530 (1% SDS, 10 mM EDTA, 50 mM Tris-HCl, pH 8 with protease inhibitor cocktail) and the lysate
531 was syringe-passaged through a 27 gauge needle. The cell lysates were sonicated using a
532 Covaris ME220 (peak power 75, duty factor 25 %, 500 cycles per burst) for 10 min for Menin,
533 NPM1c and MLL-N ChIP, or for 5 min for histone ChIP. The sonicated lysates were pre-
534 cleared with a 1:1 mix of Protein A:Protein G beads for 15 minutes at 4˚C, then incubated with
535 antibody overnight. Antibodies are provided in **Supplementary Table 1**. Five percent of the
536 lysate was set aside as input. The following day, a 1:1 mix of Protein A:Protein G beads was
537 added to each IP and samples were rotated at 4 ˚C for 3 hours. The beads were then washed
538 three times with RIPA buffer (50 mM HEPES-KOH, pH 7.6, 500 mM LiCl, 1 mM EDTA, 1%
539 NP-40, 0.7% Na-deoxycholate) and once with TE/50 mM NaCl. The chromatin was eluted
540 from the beads with SDS lysis buffer for 30 min at 65 ºC, then treated with RNase A for 30 min
541 at 37 ºC, followed by Proteinase K treatment combined with cross-link reversal overnight at
542 65 ºC. DNA was purified using the ChIP DNA Clean & Concentrator kit (Zymo 5201). Libraries
543 for sequencing were prepared using the NEBNext Ultra II library prep kit (E7645) and
544 sequenced by 40 bp paired-end sequencing with a NextSeq500 (Illumina).
545
546 **ATAC-seq**
547 ATAC-seq was performed as described by Buenrostro *et al*[71]. 50,000 cells were lysed in 50
548 µL cold lysis buffer (10 mM Tris-HCl pH 7.4, 10 mM NaCl, 3 mM MgCl2, 0.1 % IGEPAL CA-
549 630) and centrifuged at 500 g for 10 minutes at 4°C. The pellet was resuspended in
550 transposase buffer (1X Illumina Tagment DNA Buffer - 20034197) with 2.5 µL Tn5
551 Transposase enzyme and incubated for 30 min at 37°C. Transposed DNA was extracted using
552 the MinElute PCR Purification Kit (Qiagen 28004) following the manufacturer's instructions,
553 then PCR-amplified using Nexterra indices and NebNext Ultra II Q5 MasterMix (NEB M0544S)
554 for a total of 12 cycles. Amplified tagmented DNA was purified with the MinElute PCR
555 Purification Kit and sequenced by 75 bp paired-end sequencing.
556
557 **Transient Transcriptome RNA-sequencing (TT-seq)**
558 TT-seq was performed as previously described[72]. In triplicate, 4-5x10^7 cells were labelled with
559 500 µM 4-thiouridine (Sigma) for 5 min. 50 ng spike-in RNA, consisting of three 4-thiouridine-
560 labelled transcripts from a CAS9-encoding vector, was added to each replicate. Total RNA
561 was extracted with either Trizol or RNeasy Maxi kit (Qiagen), DNase I-treated, and fragmented
562 by sonication on Covaris ME220 for 10 s (peak power 70 W, duty factor 20%, 1000

563 cycles/burst). 150-200 µg input RNA was labelled with EZ-Link HPDP-Biotin (Pierce 21341)
564 for 90 min and purified by chloroform/isoamylalcohol extraction. Labelled RNA (i.e. nascent
565 transcripts) was isolated using the uMACS Streptavidin Kit (Miltenyi 130-074-101) following
566 the manufacturer's instructions and purified with the RNeasy MinElute Cleanup Kit (Qiagen
567 74204). cDNA synthesis and library preparation for sequencing were performed using the
568 NEBNext Ultra II Directional RNA Library Prep Kit (NEB E7760) following the protocol for
569 purified mRNA. The libraries were quantified using the KAPA Library Quantification Kit (Roche
570 KK4824) and sequenced by 80 bp paired-end sequencing or 150 bp paired-end sequencing
571 with a NextSeq500 (Illumina).
572
573 **ChIPmentation**
574 ChIPmentation was performed as previously described[73]. Protein A magnetic beads were
575 conjugated with 1.5 µg of antibody for 4 hours at 4 °C with rotation in 150 µL PBS 0.5% BSA
576 1 x protease inhibitor cocktail (PIC). Antibodies are provided in **Supplementary Table 1.** Cells
577 were fixed as for ChIP-seq. Fixed cells were lysed in 120 µL Lysis Buffer (50 mM Tris-HCl pH
578 8.0, 0.5% SDS, 10 mM EDTA, 1x protease inhibitor cocktail (PIC) and sonicated using Covaris
579 ME220 using the same conditions as for ChIP-seq to generate 200-300 bp fragments. Triton-
580 X100 was added to the sonicated chromatin to a final concentration of 1% and incubated for
581 10 min at room temperature to neutralize the lysis buffer SDS. The chromatin was pre-cleared
582 with protein A beads for 30 minutes at 4 °C with rotation. Antibody-conjugated beads were
583 washed with 150 µL PBS 0.5% FBS, then added to the pre-cleared chromatin and incubated
584 overnight at 4 °C with rotation. The following day the beads were washed three times with
585 RIPA buffer (as in ChIP-seq), once with Tris-EDTA and once with 10 mM Tris-HCl pH 8.0. The
586 beads were then resuspended in Tagmentation Buffer (10 mM Tris-HCl pH 8.0, 5 mM $MgCl_2$,
587 10% dimethylformamide) with 1 µL Tn5 transposase (Illumina). Samples were incubated at 37
588 °C for 5 minutes, after which the transposition reaction was stopped with 150 µL RIPA buffer.
589 Beads were washed with 10 mM Tris-HCl pH 8.0. PCR was performed with NEBNext Ultra II
590 Q5 Mastermix and Nextera index primers (125 nM final concentration) for 13 cycles. AMPure
591 XP beads (Beckman A63881) in a 1:1 ratio were used for clean-up. Samples were sequenced
592 with paired-end sequencing with a NextSeq500 (Illumina).
593
594 **Immunoprecipitation**
595 $4x10^7$ cells were lysed in 1 mL Buffer A (10 mM HEPES pH 7.9, 10 mM KCl, 1.5 mM $MgCl_2$,
596 0.34 M sucrose, 10% glycerol) with 0.2% NP-40 and 1x PIC for 5 minutes on ice. Following a
597 5 minute centrifugation at 500g and 4 °C, the cytoplasmic fraction (supernatant) was removed
598 and intact nuclei were washed once in Buffer A + PIC. The nuclei were resuspended in Nuclear
599 Lysis Buffer (50 mM Tris-HCl, pH 8, 2 mM $MgCl_2$, 150 mM NaCl, 0.5% NP-40, 1x PIC) with

600 250 U benzonase (Sigma) and rotated for 1 h at 4 ˚C. For cells treated with 250 nM MENi for
601 24 h, all buffers were supplemented with VTP50469 to 1mM. After centrifugation at 20,000 g
602 for 10 min and 4 °C, 2% of the supernatant was set aside as a nuclear input and the remainder
603 was used for immunoprecipitation with 4 µg anti-Menin antibody (Bethyl A300-105A) overnight
604 at 4 °C. An equal amount of rabbit IgG antibody (Cell Signalling DA1E) was used in parallel
605 as a control. A 1:1 mix of Protein A:Protein G beads was added to each IP and rotated at 4 °C
606 for 3 h. The beads were washed three times with Nuclear Lysis Buffer and once with TE/50
607 mM NaCl. The beads were then resuspended in 35 µL 2X LDS buffer and proteins were eluted
608 by incubating at 95 °C for 5 min. For quality checks, approximately 4% of the sample was used
609 for SDS-PAGE followed by Silver Stain (Pierce™ Silver Stain Kit, ThermoFisher 24612) and
610 8.5% was used for western blotting for LEDGF, a protein known to interact with Menin.
611
612 **Mass Spectrometry**
613 Peptides were prepared for Mass Spectrometry with the S-trap micro spin column digestion
614 protocol (PROTIFI), following the manufacturer's instructions. Briefly, samples were reduced,
615 alkylated and acidified, then purified with the S-Trap micro column. After 5 washes with the
616 binding/wash buffer, 5 µg Trypsin was added and columns were incubated at 37 °C overnight.
617 Peptides were resuspended in 5% formic acid and 5% DMSO and then trapped on an
618 Acclaim™ PepMap™ 100 C18 HPLC Columns (PepMapC18; 300µm x 5mm, 5µm particle
619 size, Thermo Fischer) using solvent A (0.1% Formic Acid in water) at a pressure of 60 bar and
620 separated on an Ultimate 3000 UHPLC system (Thermo Fischer Scientific) coupled to a
621 QExactive mass spectrometer (Thermo Fischer Scientific). The peptides were separated on
622 an Easy Spray PepMap RSLC column (75µm i.d. x 2µm x 50mm, 100 Å, Thermo Fisher) and
623 then electro-sprayed directly into an QExactive mass spectrometer (Thermo Fischer Scientific)
624 through an EASY-Spray nano-electrospray ion source (Thermo Fischer Scientific) using a
625 linear gradient (length: 60 minutes, 5% to 35% solvent B (0.1% formic acid in acetonitrile and
626 5% dimethyl sulfoxide), flow rate: 250 nL/min). The raw data was acquired in the mass
627 spectrometer in a data-independent mode (DIA). Full scan MS spectra were acquired in the
628 Orbitrap (inclusion list with scan range 495 to 995 m/z, 20m/z increments, with an overlap of
629 +/- 2 Daltons, resolution 35000, AGC target 3e6, maximum injection time 55ms). After the MS
630 scans peaks were selected for HCD fragmentation at 28% of normalised collision
631 energy(NCE) / stepped NCE. HCD spectra were also acquired in the Orbitrap (resolution
632 17500, AGC target 1e6, isolation window 20m/z).
633
634 **Micro-Capture-C**
635 Micro-Capture-C was conducted as previously[52,74]. In triplicate, $5x10^7$ SEM and OCI-AML3
636 cells were treated with 250 nM VTP50469 or DMSO for 24 hours. Cells were fixed with 2%

637 formaldehyde for 10 min, followed by quenching with glycine and a PBS wash. Cells were
638 then aliquoted into three technical replicates. 0.0005% digitonin (Sigma) was used to
639 permeabilize the cells for 15 minutes, after which they were snap frozen in three aliquots.
640 After thawing, 16 x 10^6 cells (one aliquot) were resuspended in 10mM Tris-HCl pH 7.5, 1 mM
641 $CaCl_2$ and divided into three micrococcal nuclease (NEB) digestion reactions with 7.5, 10 or
642 12.5 Kunitz U for 1 h at 37 °C shaking at 550 rpm in a Thermomixer (Eppendorf). MNase
643 digestion was stopped with 5 mM EGTA and an aliquot was set aside to assess digestion by
644 TapeStation. The cells were washed with PBS/5 mM EGTA and resuspended in: DNA ligase
645 buffer, 400 µM dNTPs, 5 mM EDTA, 100 U/µL DNA Polymerase 1, Large (Klenow)
646 Fragment (NEB), 200 U/µL T4 PNK (NEB) and 300 U/µL T4 DNA ligase (Thermo Scientific).
647 This ligation reaction was incubated at 550 rpm at 37 °C for 2 h followed by 20 °C for 8
648 hours, then held at 4 °C in a ThermoMixer. Cells were then washed with PBS and digested
649 with Proteinase K at 65 °C overnight to simultaneously reverse crosslinks. DNA was purified
650 using phenol:chloroform:isoamyl alcohol (25:24:1) and digestion and ligation were assessed
651 by TapeStation (Agilent D1000). 3C libraries (two technical replicates per biological
652 replicate) were sonicated to 200 bp on Covaris ME220. Indexing was performed in duplicate
653 using Illumina paired-end adaptors, NEB Indices and Herculase II (Agilent). Enrichment for
654 promoters of interest was performed twice with 120 nt biotinylated capture probes using the
655 HyperCapture Target Enrichment Kit (Roche), using M270 streptavidin beads (Invitrogen) for
656 the pulldown. Capture probes were designed using the Capsequm pipeline
657 (https://github.com/Davies-Genomics-and-Genome-Editing-Lab/oligo_design_pipeline).
658 Sequences are provided in Supplementary File 1. Samples were sequenced by 150 bp
659 paired-end sequencing on NextSeq500 (Illumina).
660
661 **Bioinformatic analysis**
662
663 Publicly available genomics data was accessed from GEO. References to the data are
664 provided in **Supplementary Table 2**.
665
666 **ChIP-seq and ChIPmentation.** Sequencing reads were trimmed using trim_galore
667 (https://github.com/FelixKrueger/TrimGalore) and aligned to hg38 using bowtie2.[75]
668 DeepTools[76] was used to create bigwig files for visualization on UCSC and to generate
669 heatmaps and metaplots. HOMER[77] was used to call peaks using findPeaks and the flag -
670 style histone. ChIP-seq signal at peaks was quantified using the deepTools command
671 multiBigwigSummary BED-file. Differential peak analysis was performed with the R package
672 DiffBind.[78] Heatmaps of differential peaks were generated with R package
673 ComplexHeatmap.[79]

674

675 **TT-seq.** Transient transcriptome RNA sequencing reads were aligned to human genome
676 (hg38) using STAR,[80] and gene expression levels were determined using the Subread
677 package tool featureCounts. [81] Differential gene expression analysis was completed using
678 edgeR.[82] Metaplot visualisations of strand-specific transcription were created using the
679 deepTools command computeMatrix and plotted in R using ggplot2. χ^2 tests were performed
680 using the R package ggstatsplot.[83]
681
682 **Genomic annotation.** ATAC, ChIP-seq and ChIPmentation peaks were annotated with the R
683 package ChIPseeker.[84] Promoters were defined as ATAC-seq peaks that overlap H3K27ac
684 peaks and are within 2 kb of an annotated transcription start site (TSS). Enhancers were
685 defined as ATAC-seq peaks that overlap H3K27ac peaks and are 2 kb or more away from an
686 annotated TSS. In heatmaps and metaplots depicting enhancers, ChIP-seq signal was
687 centred on the enhancer ATAC peak for cell lines. For patient samples missing ATAC data,
688 the ChIP-seq signal was centred on H3K27ac peaks. Enhancers were assigned to genes
689 using the nearest annotated TSS.
690
691 **Immunoprecipitation Mass Spectrometry.** Data search was performed in a library-free
692 search in DIA-NN[85] 1.8.1 with the database UPR UPR_Homo
693 sapiens_9606_UP000005640_20200803.fasta. FDR (false discovery rate) was set to 0.01
694 and MBR (match between runs) was enabled. Mass spec intensities were normalized by
695 MaxLFQ (generic label free technology) and transformed to log2. Imputation was performed
696 in R by replacing missing values with randomly sampled values from a down-shifted normal
697 distribution following methods described in [86]. Keratins and common contaminants identified
698 in 95% of the CRAPome database[87] were excluded from the data. Comparisons between
699 conditions (IgG and Menin IPs) were performed with moderated t-tests using the R package
700 Genoppi[88] (https://github.com/lagelab/Genoppi) and corrected for multiple comparisons using
701 False Discovery Rate with the R package fdrtools.[89] Volcano plots were generated using
702 ggplot2. Enrichment analyses were performed with a hypergeometric test from the Genoppi
703 package using the CORUM database.[58]
704
705 **Micro-Capture-C.** Analysis was performed using the Micro-Capture-C pipeline from the
706 Davies lab (https://github.com/jojdavies/Micro-Capture-C). Peak calling was performed with
707 deep-learning-based peak caller LanceOtron.[90] The peaks were filtered using a custom script
708 from the Davies Lab based on size, width, and distance from the capture viewpoint. Unique
709 junctions were counted at each MCC peak, then normalized using cis unique ligation junctions
710 for the corresponding viewpoint as previously reported.[52] Junctions were compared between

conditions using a Mann-Whitney U test corrected for multiple comparisons using R package fdrtools, and comparisons were visualized in R using ggplot2. MCC peaks were intersected with Menin ChIP-seq peaks using bedtools intersect. Pearson's chi-square test was used to test for independence between Menin peaks and differential MCC peaks.

For patient sample MCC (Figure 4), MCC peaks were intersected with Homer Menin peaks that were within 2 Mb centered on the capture viewpoint (± 1mB each side), excluding ± 2 kb region around the center of the viewpoint. LancoTron MCC peaks often failed to capture the entirety of broad Menin-bound enhancers; as a result, unique ligation junctions were counted over Menin peaks that intersected with MCC peaks, specific to each patient. Each patient had a unique set of MCC (4 technical replicates per condition) and Menin peaks (1 replicate per condition) and were treated independently. Log2 fold changes in ligation junction counts were computed per peak for each patient using the average counts from 4 technical replicates.

Genomic track visualization

BigWigs were visualized in the UCSC Genome Browser (genome.ucsc.edu). The signal visualized is the mean or mean + whiskers (1 standard deviation, and maximum/minimum) where indicated. Subtraction plots are smoothed to 10 pixels.

Use of Artificial Intelligence

ChatGPT Edu was used for troubleshooting and optimizing bash and R code generated by the authors. AI was not used in writing the manuscript.

735 **References**

736

737 1. Strahl BD, Allis CD. The language of covalent histone modifications. *Nature*.
738 2000;403(6765):41-45.
739 2. Dawson MA, Kouzarides T. Cancer epigenetics: From mechanism to therapy. *Cell*.
740 2012;150(1):12-27.
741 3. Bhagwat AS, Lu B, Vakoc CR. Enhancer dysfunction in leukemia. *Blood*.
742 2018;131(16):1795.
743 4. Siklos M, Kubicek S. Therapeutic targeting of chromatin: status and opportunities.
744 *FEBS J*. 2022;289(5):1276-1301.
745 5. Cheng Y, He C, Wang M, et al. Targeting epigenetic regulators for cancer therapy:
746 mechanisms and advances in clinical trials. *Signal Transduction and Targeted*
747 *Therapy 2019 4:1*. 2019;4(1):1-39.
748 6. Mabe NW, Perry JA, Malone CF, Stegmaier K. Pharmacological targeting of the
749 cancer epigenome. *Nature Cancer 2024 5:6*. 2024;5(6):844-865.
750 7. Brown MR, Soto-Feliciano YM. Menin: from molecular insights to clinical impact.
751 *Epigenomics*. 2025;17(7):489-505.
752 8. Balogh K, Rácz K, Patócs A, Hunyady L. Menin and its interacting proteins:
753 elucidation of menin function. *Trends in Endocrinology and Metabolism*.
754 2006;17(9):357-364.
755 9. Matkar S, Thiel A, Hua X. Menin: a scaffold protein that controls gene expression and
756 cell signaling. *Trends Biochem Sci*. 2013;38(8):394-402.
757 10. Balogh K, Patócs A, Hunyady L, Rácz K. Menin dynamics and functional insight: Take
758 your partners. *Mol Cell Endocrinol*. 2010;326(1-2):80-84.
759 11. Issa GC, Aldoss I, DiPersio J, et al. The menin inhibitor revumenib in KMT2A-
760 rearranged or NPM1-mutant leukemia. *Nature*. 2023;615(7954):920-924.
761 12. Borkhardt A, Wuchter C, Viehmann S, et al. Infant acute lymphoblastic leukemia -
762 combined cytogenetic, immunophenotypical and molecular analysis of 77 cases.
763 *Leukemia*. 2002;16(9):1685-1690.
764 13. Rice S, Roy A. MLL-rearranged infant leukemia: A “thorn in the side” of a remarkable
765 success story. *Biochim Biophys Acta Gene Regul Mech*. 2020;1863(8).
766 14. Winters AC, Bernt KM. MLL-Rearranged Leukemias-An Update on Science and
767 Clinical Approaches. *Front Pediatr*. 2017;5:4.
768 15. Meyer C, Burmeister T, Gröger D, et al. The MLL recombinome of acute leukemias in
769 2017. *Leukemia*. 2018;32(2):273-284.

770 16. Takahashi S, Yokoyama A. The molecular functions of common and atypical MLL
771 fusion protein complexes. *Biochimica et Biophysica Acta (BBA) - Gene Regulatory*
772 *Mechanisms*. 2020;1863(7):194548.
773 17. Basu S, Nandy A, Biswas D. Keeping RNA polymerase II on the run: Functions of
774 MLL fusion partners in transcriptional regulation. *Biochim Biophys Acta Gene Regul*
775 *Mech*. 2020;1863(8).
776 18. Slany RK. MLL fusion proteins and transcriptional control. *Biochimica et Biophysica*
777 *Acta (BBA) - Gene Regulatory Mechanisms*. 2020;1863(3):194503.
778 19. Yokoyama A, Wang Z, Wysocka J, et al. Leukemia Proto-Oncoprotein MLL Forms a
779 SET1-Like Histone Methyltransferase Complex with Menin To Regulate Hox Gene
780 Expression. *Mol Cell Biol*. 2004;24(13):5639-5649.
781 20. Grembecka J, He S, Shi A, et al. Menin-MLL inhibitors reverse oncogenic activity of
782 MLL fusion proteins in leukemia. *Nat Chem Biol*. 2012;8(3):277-284.
783 21. Uckelmann HJ, Haarer EL, Takeda R, et al. Mutant NPM1 Directly Regulates
784 Oncogenic Transcription in Acute Myeloid Leukemia. *Cancer Discov*. 2023;13(3):746-
785 765.
786 22. Klossowski S, Miao H, Kempinska K, et al. Menin inhibitor MI-3454 induces remission
787 in MLL1-rearranged and NPM1-mutated models of leukemia. *Journal of Clinical*
788 *Investigation*. 2020;130(2):981-997.
789 23. Uckelmann HJ, Kim SM, Wong EM, et al. Therapeutic targeting of preleukemia cells
790 in a mouse model of NPM1 mutant acute myeloid leukemia. *Science (1979)*.
791 2020;367(6477):586-590.
792 24. Wang XQD, Fan D, Han Q, et al. Mutant NPM1 Hijacks Transcriptional Hubs to
793 Maintain Pathogenic Gene Programs in Acute Myeloid Leukemia. *Cancer Discov*.
794 2023;13(3):724-745.
795 25. Kühn MWM, Song E, Feng Z, et al. Targeting chromatin regulators inhibits
796 leukemogenic gene expression in NPM1 mutant leukemia. *Cancer Discov*.
797 2016;6(10):1166-1181.
798 26. Rau R, Brown P. Nucleophosmin (NPM1) mutations in adult and childhood acute
799 myeloid leukemia: Towards definition of a new leukemia entity. *Hematol Oncol*.
800 2009;27(4):171-181.
801 27. Ranieri R, Pianigiani G, Sciabolacci S, et al. Current status and future perspectives in
802 targeted therapy of NPM1-mutated AML. *Leukemia*. 2022;36(10):2351.
803 28. Bolli N, Nicoletti I, De Marco MF, et al. Born to be exported: COOH-terminal nuclear
804 export signals of different strength ensure cytoplasmic accumulation of
805 nucleophosmin leukemic mutants. *Cancer Res*. 2007;67(13):6230-6237.

806 29. Falini B, Bolli N, Shan J, et al. Both carboxy-terminus NES motif and mutated
807 tryptophan(s) are crucial for aberrant nuclear export of nucleophosmin leukemic
808 mutants in NPMc+ AML. *Blood*. 2006;107(11):4514-4523.
809 30. Falini B, Mecucci C, Tiacci E, et al. Cytoplasmic nucleophosmin in acute
810 myelogenous leukemia with a normal karyotype. *N Engl J Med*. 2005;352(3):254-266.
811 31. Alcalay M, Tiacci E, Bergomas R, et al. Acute myeloid leukemia bearing cytoplasmic
812 nucleophosmin (NPMc+ AML) shows a distinct gene expression profile characterized
813 by up-regulation of genes involved in stem-cell maintenance. *Blood*. 2005;106(3):899-
814 902.
815 32. Brunetti L, Gundry MC, Sorcini D, et al. Mutant NPM1 Maintains the Leukemic State
816 through HOX Expression. *Cancer Cell*. 2018;34(3):499-512.e9.
817 33. Krivtsov A V., Evans K, Gadrey JY, et al. A Menin-MLL Inhibitor Induces Specific
818 Chromatin Changes and Eradicates Disease in Models of MLL-Rearranged
819 Leukemia. *Cancer Cell*. 2019;36(6):660-673.e11.
820 34. Kerry J, Godfrey L, Repapi E, et al. MLL::AF4 Spreading Identifies Binding Sites that
821 Are Distinct from Super-Enhancers and that Govern Sensitivity to DOT1L Inhibition in
822 Leukemia. *Cell Rep*. 2017;18(2):482-495.
823 35. Prange KHM, Mandoli A, Kuznetsova T, et al. MLL-AF9 and MLL::AF4 oncofusion
824 proteins bind a distinct enhancer repertoire and target the RUNX1 program in 11q23
825 acute myeloid leukemia. *Oncogene*. 2017;36(23):3346-3356.
826 36. Crump NT, Smith AL, Godfrey L, et al. MLL::AF4 cooperates with PAF1 and FACT to
827 drive high-density enhancer interactions in leukemia. *Nat Commun*. 2023;14(1):5208.
828 37. Godfrey L, Crump NT, Thorne R, et al. DOT1L inhibition reveals a distinct subset of
829 enhancers dependent on H3K79 methylation. *Nature Communications 2019 10:1*.
830 2019;10(1):1-15.
831 38. Panigrahi A, O'Malley BW. Mechanisms of enhancer action: the known and the
832 unknown. *Genome Biol*. 2021;22(1):108.
833 39. Smith AL, Denny N, Chahrour C, et al. Enhancer heterogeneity in acute lymphoblastic
834 leukemia drives differential gene expression in patients. *Blood*. 2025;146(17).
835 40. Pan F, Iwasaki M, Wu W, et al. Enhancer remodeling drives MLL oncogene-
836 dependent transcriptional dysregulation in leukemia stem cells. *Blood Adv*.
837 2023;7(11):2504-2519.
838 41. Dreijerink KMA, Groner AC, Vos ESM, et al. Enhancer-Mediated Oncogenic Function
839 of the Menin Tumor Suppressor in Breast Cancer. *Cell Rep*. 2017;18(10):2359-2372.
840 42. Sun J, Yu W, Zhang X. MENIN inhibitor-based therapy in acute leukemia: latest
841 updates from the 2024 ASH annual meeting. *Exp Hematol Oncol*. 2025;14(1):1-4.

842 43. Candoni A, Coppola G. A 2024 Update on Menin Inhibitors. A New Class of Target
843 Agents against KMT2A-Rearranged and NPM1-Mutated Acute Myeloid Leukemia.
844 *Hematol Rep*. 2024;16(2):244.
845 44. Freire PR, Cutler JA, Armstrong SA. Therapeutic Targeting of the Menin–KMT2A
846 Interaction. *Annu Rev Cancer Biol*. 2024;8(1):291-307.
847 45. Milne TA, Dou Y, Martin ME, Brock HW, Roeder RG, Hess JL. MLL associates
848 specifically with a subset of transcriptionally active target genes. *Proc Natl Acad Sci U*
849 *S A*. 2005;102(41):14765-14770.
850 46. Okuda H, Kawaguchi M, Kanai A, et al. MLL fusion proteins link transcriptional
851 coactivators to previously active CpG-rich promoters. *Nucleic Acids Res*.
852 2014;42(7):4241-4256.
853 47. Janssens DH, Meers MP, Wu SJ, et al. Automated CUT&Tag profiling of chromatin
854 heterogeneity in mixed-lineage leukemia. *Nature Genetics 2021 53:11*.
855 2021;53(11):1586-1596.
856 48. Schmidl C, Rendeiro AF, Sheffield NC, Bock C. ChIPmentation: fast, robust, low-input
857 ChIP-seq for histones and transcription factors. *Nat Methods*. 2015;12(10):963-965.
858 49. Chen H, Levo M, Barinov L, Fujioka M, Jaynes JB, Gregor T. Dynamic interplay
859 between enhancer–promoter topology and gene activity. *Nature Genetics 2018 50:9*.
860 2018;50(9):1296-1303.
861 50. Brown JM, Roberts NA, Graham B, et al. A tissue-specific self-interacting chromatin
862 domain forms independently of enhancer-promoter interactions. *Nature*
863 *Communications 2018 9:1*. 2018;9(1):1-15.
864 51. Nollmann M, Bennabi I, Götz M, Gregor T. The Impact of Space and Time on the
865 Functional Output of the Genome. *Cold Spring Harb Perspect Biol*.
866 2022;14(4):a040378.
867 52. Hua P, Badat M, Hanssen LLP, et al. *Defining Genome Architecture at Base-Pair*
868 *Resolution*. Vol 595. Springer US; 2021.
869 53. Mueller D, Bach C, Zeisig D, et al. A role for the MLL fusion partner ENL in
870 transcriptional elongation and chromatin modification. *Blood*. 2007;110(13):4445-
871 4454.
872 54. Orphanides G, LeRoy G, Chang CH, Luse DS, Reinberg D. FACT, a factor that
873 facilitates transcript elongation through nucleosomes. *Cell*. 1998;92(1):105-116.
874 55. Kim J, Guermah M, Roeder RG. The human PAF1 complex acts in chromatin
875 transcription elongation both independently and cooperatively with SII/TFIIS. *Cell*.
876 2010;140(4):491-503.

877 56. Raisner R, Kharbanda S, Jin L, et al. Enhancer Activity Requires CBP/P300
878 Bromodomain-Dependent Histone H3K27 Acetylation. *Cell Rep*. 2018;24(7):1722-
879 1729.
880 57. Hogg SJ, Motorna O, Cluse LA, et al. Targeting histone acetylation dynamics and
881 oncogenic transcription by catalytic P300/CBP inhibition. *Mol Cell*. 2021;81(10):2183-
882 2200.e13.
883 58. Tsitsiridis G, Steinkamp R, Giurgiu M, et al. CORUM: the comprehensive resource of
884 mammalian protein complexes–2022. *Nucleic Acids Res*. 2023;51(D1):D539-D545.
885 59. Meyers RM, Bryan JG, McFarland JM, et al. Computational correction of copy number
886 effect improves specificity of CRISPR–Cas9 essentiality screens in cancer cells.
887 *Nature Genetics 2017 49:12*. 2017;49(12):1779-1784.
888 60. Krivtsov A V., Twomey D, Feng Z, et al. Transformation from committed progenitor to
889 leukemia stem cell initiated by MLL–AF9. *Nature 2006 442:7104*.
890 2006;442(7104):818-822.
891 61. Adriaanse FRS, Schneider P, Arentsen-Peters STCJM, et al. Distinct Responses to
892 Menin Inhibition and Synergy with DOT1L Inhibition in KMT2A-Rearranged Acute
893 Lymphoblastic and Myeloid Leukemia. *Int J Mol Sci*. 2024;25(11):6020.
894 62. Perner F, Gadrey JY, Armstrong SA, Kühn MWM. Targeting the Menin–KMT2A
895 interaction in leukemia: Lessons learned and future directions. *Int J Cancer*. Published
896 online 2025.
897 63. Xu H, Valerio DG, Eisold ME, et al. NUP98-Fusion Proteins Interact With the NSL and
898 MLL1 Complexes To Drive Leukemogenesis. *Cancer Cell*. 2016;30(6):863.
899 64. Barajas JM, Rasouli M, Umeda M, et al. Acute myeloid leukemias with UBTF tandem
900 duplications are sensitive to menin inhibitors. *Blood*. 2024;143(7):619-630.
901 65. Olsen SN, Anderson B, Hatton C, et al. Combined inhibition of KAT6A/B and Menin
902 reverses estrogen receptor-driven gene expression programs in breast cancer. *Cell*
903 *Rep Med*. 2025;6(7):102192.
904 66. Hemming ML, Benson MR, Loycano MA, et al. MOZ and Menin–MLL Complexes Are
905 Complementary Regulators of Chromatin Association and Transcriptional Output in
906 Gastrointestinal Stromal Tumor. *Cancer Discov*. 2022;12(7):1804-1821.
907 67. Perner F, Stein EM, Wenge D V., et al. MEN1 mutations mediate clinical resistance to
908 menin inhibition. *Nature*. 2023;615(7954):913-919.
909 68. Pieters R, De Lorenzo P, Ancliffe P, et al. Outcome of infants younger than 1 year
910 with acute lymphoblastic leukemia treated with the interfant-06 protocol: Results from
911 an international phase III randomized study. *Journal of Clinical Oncology*.
912 2019;37(25):2246-2256.

913 69. Kaspers GJL, Veerman AJP, Pieters R, et al. Mononuclear cells contaminating acute
914 lymphoblastic leukaemic samples tested for cellular drug resistance using the methyl-
915 thiazol-tetrazolium assay. *British Journal of Cancer 1994 70:6*. 1994;70(6):1047-1052.
916 70. Ritz C, Baty F, Streibig JC, Gerhard D. Dose-Response Analysis Using R. *PLoS One*.
917 2015;10(12):e0146021.
918 71. Buenrostro JD, Wu B, Chang HY, Greenleaf WJ. ATAC-seq: A Method for Assaying
919 Chromatin Accessibility Genome-Wide. *Current protocols in molecular biology / edited*
920 *by Frederick M Ausubel . [et al]*. 2015;109:21.29.1.
921 72. Schwalb B, Michel M, Zacher B, et al. TT-seq maps the human transient
922 transcriptome. *Science (1979)*. 2016;352(6290):1225-1228.
923 73. Schmidl C, Rendeiro AF, Sheffield NC, Bock C. ChIPmentation: fast, robust, low-input
924 ChIP-seq for histones and transcription factors. *Nat Methods*. 2015;12(10):963-965.
925 74. Hamley JC, Li H, Denny N, Downes D, Davies JOJ. Determining chromatin
926 architecture with Micro Capture-C. *Nat Protoc*. 2023;18(6):1687-1711.
927 75. Langmead B, Salzberg SL. Fast gapped-read alignment with Bowtie 2. *Nature*
928 *Methods 2012 9:4*. 2012;9(4):357-359.
929 76. Ramírez F, Dündar F, Diehl S, Grüning BA, Manke T. deepTools: a flexible platform
930 for exploring deep-sequencing data. *Nucleic Acids Res*. 2014;42(W1):W187-W191.
931 77. Heinz S, Benner C, Spann N, et al. Simple Combinations of Lineage-Determining
932 Transcription Factors Prime cis-Regulatory Elements Required for Macrophage and B
933 Cell Identities. *Mol Cell*. 2010;38(4):576-589.
934 78. Stark R, Brown G. DiffBind: differential binding analysis of ChIP-Seq peak data. 2011.
935 79. Gu Z, Eils R, Schlesner M. Complex heatmaps reveal patterns and correlations in
936 multidimensional genomic data. *Bioinformatics*. 2016;32(18):2847-2849.
937 80. Dobin A, Davis CA, Schlesinger F, et al. STAR: ultrafast universal RNA-seq aligner.
938 *Bioinformatics*. 2013;29(1):15-21.
939 81. Liao Y, Smyth GK, Shi W. featureCounts: an efficient general purpose program for
940 assigning sequence reads to genomic features. *Bioinformatics*. 2014;30(7):923-930.
941 82. Robinson MD, McCarthy DJ, Smyth GK. edgeR : a Bioconductor package for
942 differential expression analysis of digital gene expression data. *Bioinformatics*.
943 2010;26(1):139-140.
944 83. Patil I. Visualizations with statistical details: The “ggstatsplot” approach. *J Open*
945 *Source Softw*. 2021;6(61):3167.
946 84. Yu G, Wang LG, He QY. ChIPseeker: an R/Bioconductor package for ChIP peak
947 annotation, comparison and visualization. *Bioinformatics*. 2015;31(14):2382-2383.

948 85. Demichev V, Messner CB, Vernardis SI, Lilley KS, Ralser M. DIA-NN: neural
949 networks and interference correction enable deep proteome coverage in high
950 throughput. *Nat Methods*. 2020;17(1):41-44.
951 86. Tyanova S, Temu T, Sinitcyn P, et al. The Perseus computational platform for
952 comprehensive analysis of (prote)omics data. *Nat Methods*. 2016;13(9):731-740.
953 87. Mellacheruvu D, Wright Z, Couzens AL, et al. The CRAPome: a Contaminant
954 Repository for Affinity Purification Mass Spectrometry Data. *Nat Methods*.
955 2013;10(8):730.
956 88. Pintacuda G, Lassen FH, Hsu YHH, et al. Genoppi is an open-source software for
957 robust and standardized integration of proteomic and genetic data. *Nat Commun*.
958 2021;12(1):1-10.
959 89. Strimmer K. fdrtool: a versatile R package for estimating local and tail area-based
960 false discovery rates. *Bioinformatics*. 2008;24(12):1461-1462.
961 90. Hentges LD, Sergeant MJ, Cole CB, Downes DJ, Hughes JR, Taylor S. LanceOtron:
962 a deep learning peak caller for genome sequencing experiments. *Bioinformatics*.
963 2022;38(18):4255-4263.
964

Figure 1

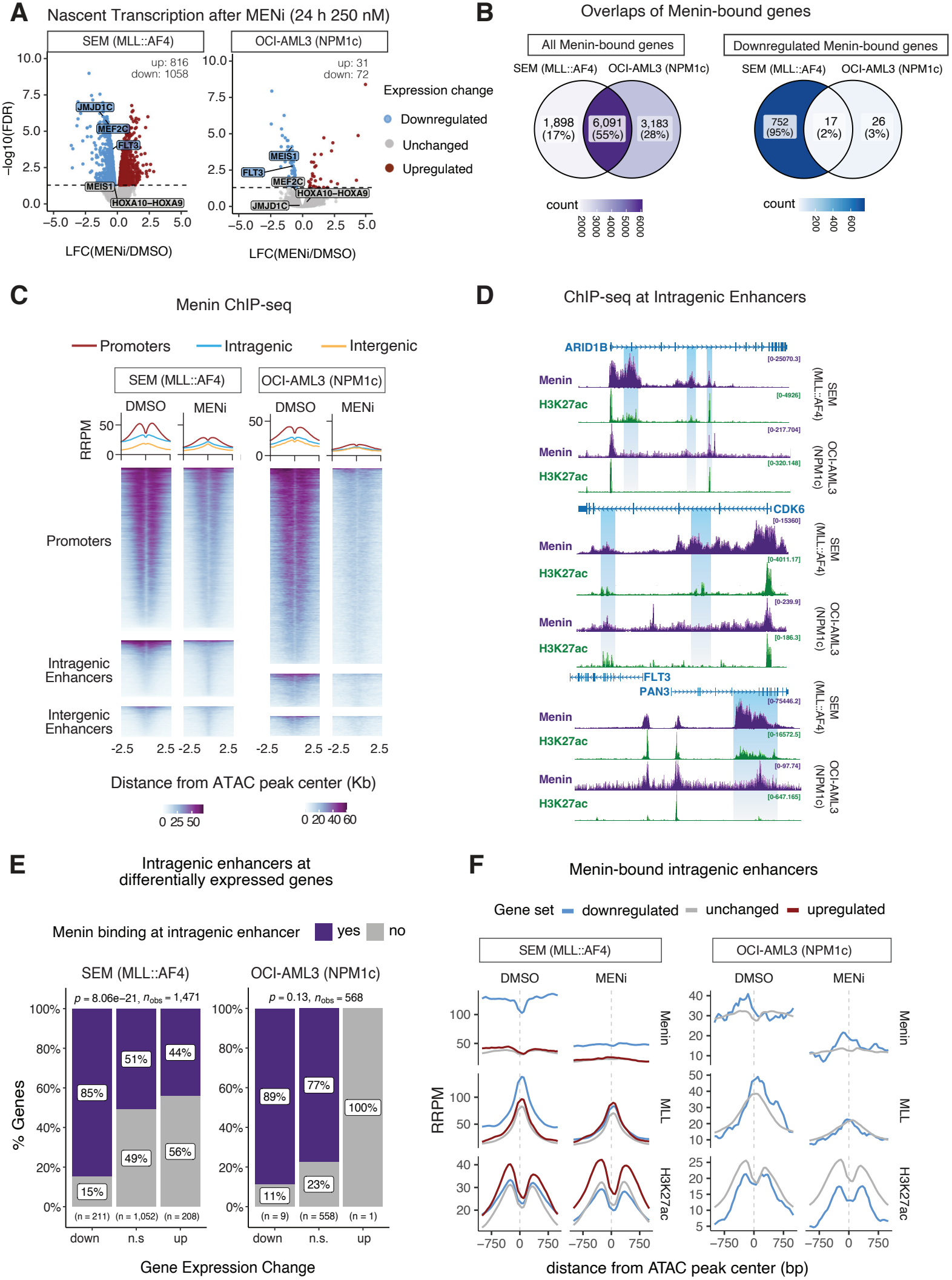
A
Nascent Transcription after MENi (24 h 250 nM)
SEM (MLL::AF4)
OCI-AML3 (NPM1c)
up: 816
down: 1058
up: 31
down: 72
−log10(FDR)
JMJD1C
MEF2C
FLT3
MEIS1
HOXA10–HOXA9
LFC(MENi/DMSO)
Expression change
Downregulated
Unchanged
Upregulated
B
Overlaps of Menin-bound genes
All Menin-bound genes
Downregulated Menin-bound genes
SEM (MLL::AF4)
OCI-AML3 (NPM1c)
1,898 (17%)
6,091 (55%)
3,183 (28%)
752 (95%)
17 (2%)
26 (3%)
count
C
Menin ChIP-seq
Promoters
Intragenic
Intergenic
DMSO
MENi
RRPM
Intragenic Enhancers
Intergenic Enhancers
Distance from ATAC peak center (Kb)
D
ChIP-seq at Intragenic Enhancers
ARID1B
CDK6
FLT3
PAN3
Menin
H3K27ac
E
Intragenic enhancers at differentially expressed genes
Menin binding at intragenic enhancer
yes
no
p = 8.06e−21, n_obs = 1,471
p = 0.13, n_obs = 568
% Genes
85%
15%
51%
49%
44%
56%
89%
11%
77%
23%
100%
(n = 211)
(n = 1,052)
(n = 208)
(n = 9)
(n = 558)
(n = 1)
down
n.s
up
Gene Expression Change
F
Menin-bound intragenic enhancers
Gene set
downregulated
unchanged
upregulated
RRPM
MLL
distance from ATAC peak center (bp)

Figure 1.: Differential effects of Menin inhibition on transcription in MLL::AF4 ALL and NPM1-mutant AML. (A) Volcano plots of transient transcriptome RNA-seq after 24 h of treatment with DMSO or 250 nM Menin inhibitor VTP50469 (MENi). (B) Overlap of all Menin-bound genes (left) and downregulated Menin-bound genes only (right) in SEM and OCI-AML3 cells. (C) Heatmaps of Menin ChIP-seq at promoters and enhancers in SEM and OCI-AML3 cells. Regions are sorted by H3K27ac signal and centered on ATAC peaks. Metaplots display the mean. (B) Examples of intragenic Menin-bound enhancers in the gene bodies of *ARID1B*, *CDK6* and *PAN3*. (D) Association between Menin binding at intragenic enhancers and altered gene expression from the nearest TSS following 24 h of MENi. *p*-values are reported from a Pearson chi-square test. (E) Mean Menin, MLL/MLL::AF4, and H3K27ac at intragenic enhancers annotated to differentially expressed genes by nearest TSS after 24 h of MENi in SEM and OCI-AML3 cells.

Figure 2

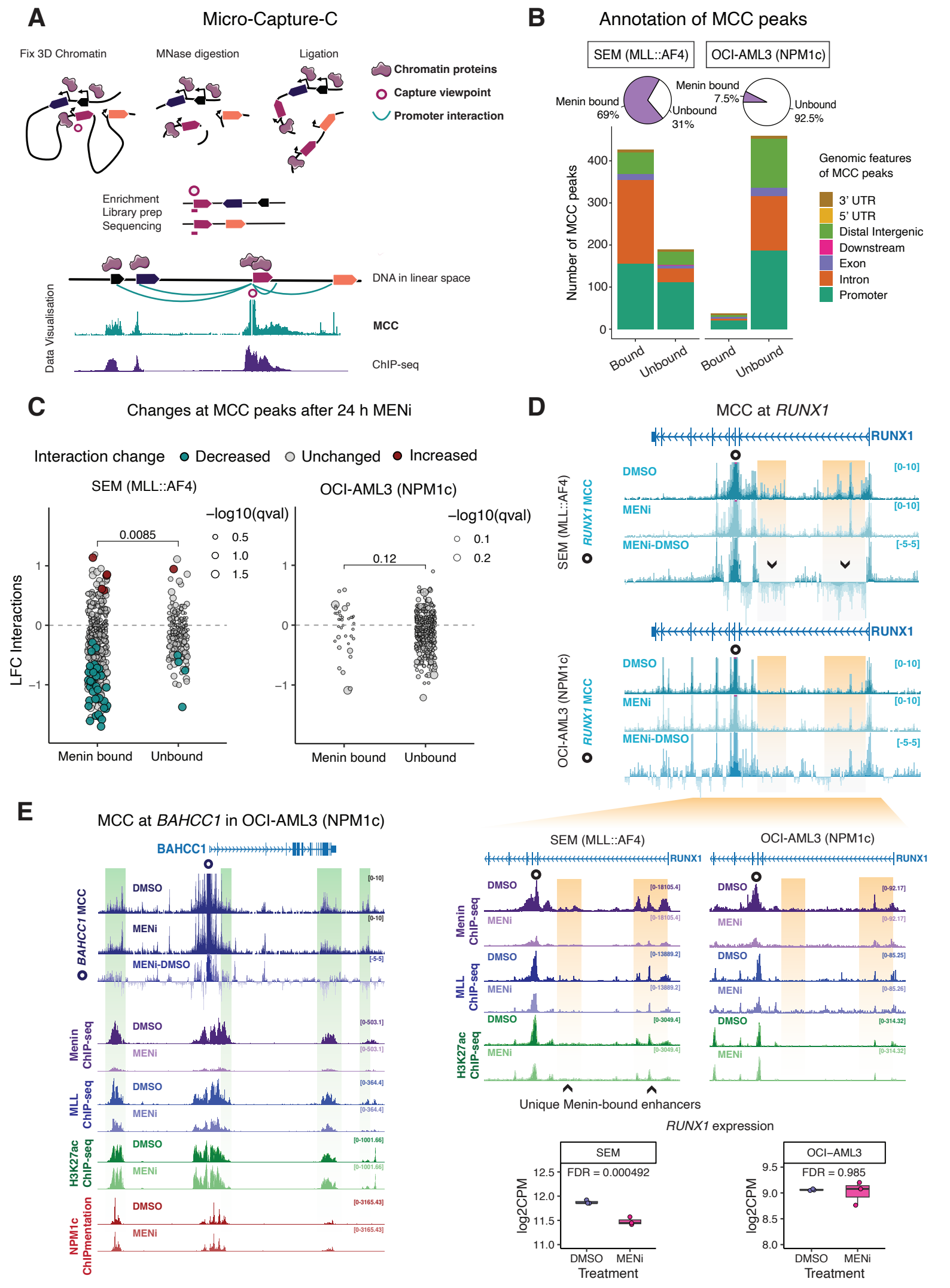
A
Micro-Capture-C
Fix 3D Chromatin
MNase digestion
Ligation
Chromatin proteins
Capture viewpoint
Promoter interaction
Enrichment
Library prep
Sequencing
DNA in linear space
MCC
ChIP-seq
Data Visualisation
B
Annotation of MCC peaks
SEM (MLL::AF4)
OCI-AML3 (NPM1c)
Menin bound 69%
Unbound 31%
Menin bound 7.5%
Unbound 92.5%
Number of MCC peaks
Genomic features of MCC peaks
3' UTR
5' UTR
Distal Intergenic
Downstream
Exon
Intron
Promoter
Bound
Unbound
C
Changes at MCC peaks after 24 h MENi
Interaction change
Decreased
Unchanged
Increased
SEM (MLL::AF4)
OCI-AML3 (NPM1c)
−log10(qval)
0.5
1.0
1.5
0.1
0.2
0.0085
0.12
LFC Interactions
Menin bound
Unbound
D
MCC at RUNX1
RUNX1
DMSO
MENi
MENi-DMSO
SEM (MLL::AF4)
OCI-AML3 (NPM1c)
RUNX1 MCC
E
MCC at BAHCC1 in OCI-AML3 (NPM1c)
BAHCC1
BAHCC1 MCC
Menin ChIP-seq
MLL ChIP-seq
H3K27ac ChIP-seq
NPM1c ChIPmentation
Unique Menin-bound enhancers
RUNX1 expression
FDR = 0.000492
FDR = 0.985
log2CPM
Treatment

Figure 2.: Menin inhibition disrupts enhancer-promoter contacts in MLL::AF4 cells but not NPM1c cells. (A) Schematic representation of Micro-Capture-C data. (B) Annotation of MCC peaks (enhancer-promoter contacts), grouped by the presence of Menin binding, in SEM and OCI-AML3 cells. (C) Changes in mean unique ligation junction counts at MCC peaks in SEM (left) and OCI-AML3 (right) cells treated with MENi (250 nM, 24 h), categorised by Menin binding. Colored data points represent significantly altered contacts (Mann-Whitney U, FDR-adjusted q-value < 0.05). *p*-values comparing bound and unbound sites are reported from a Wilcoxon test. (D) Visualization of MCC (top, mean+whiskers signal for DMSO and MENi), ChIP-seq (middle, mean signal), and gene expression (bottom, TT-seq data) at the *RUNX1* locus in SEM and OCI-AML3 cells. The MENi-DMSO subtraction track shows the difference in MCC signal (mean with whiskers) between conditions. Menin-bound enhancers in SEM cells are highlighted in yellow. (E) Visualization of MCC (top, mean+whiskers) and ChIP-seq (bottom, mean signal) at the *BAHCC1* locus in OCI-AML3 cells. Menin-bound enhancers are highlighted in green.

Figure 3

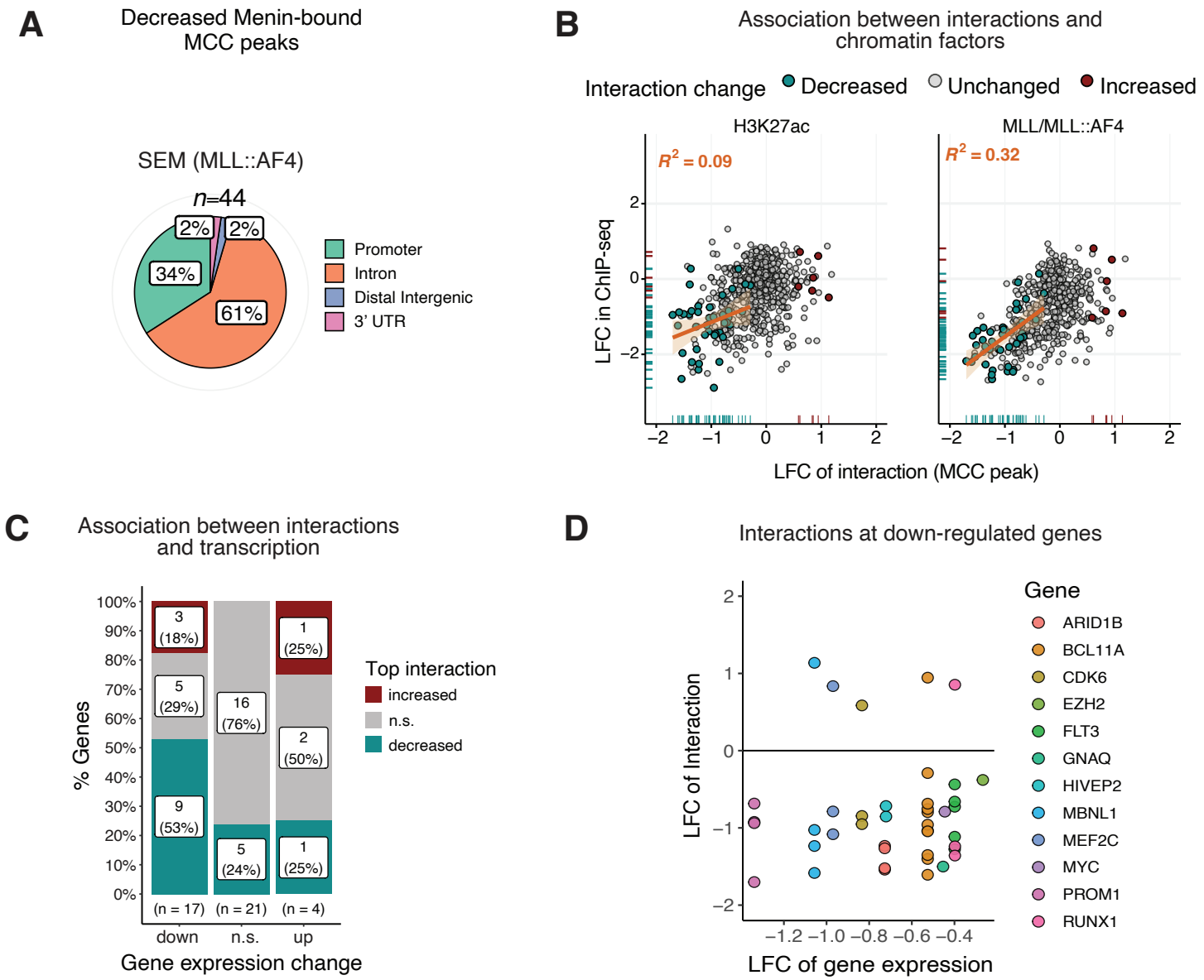
A
Decreased Menin-bound MCC peaks
SEM (MLL::AF4)
n=44
2%
2%
34%
61%
Promoter
Intron
Distal Intergenic
3' UTR
B
Association between interactions and chromatin factors
Interaction change
Decreased
Unchanged
Increased
H3K27ac
MLL/MLL::AF4
R2 = 0.09
R2 = 0.32
LFC in ChIP-seq
LFC of interaction (MCC peak)
C
Association between interactions and transcription
% Genes
3 (18%)
5 (29%)
9 (53%)
16 (76%)
5 (24%)
1 (25%)
2 (50%)
1 (25%)
(n = 17)
(n = 21)
(n = 4)
down
n.s.
up
Gene expression change
Top interaction
increased
n.s.
decreased
D
Interactions at down-regulated genes
LFC of Interaction
LFC of gene expression
Gene
ARID1B
BCL11A
CDK6
EZH2
FLT3
GNAQ
HIVEP2
MBNL1
MEF2C
MYC
PROM1
RUNX1

Figure 3.: Collapse of Menin-bound enhancers is associated with decreased transcription at key genes. (A) Annotation of decreased Menin-bound enhancers in SEM cells. (B) Scatter plots showing the change in interaction frequency correlated with the change in H3K27ac or MLL/MLL::AF4 enrichment after 24 h of MENi (250 nM) in SEM cells. Colored data points are sites with a significant (MWU FDR q-value < 0.05) change in interaction. A linear fit (orange line) is shown specifically for sites of decreased interaction. (C) Association between gene expression and enhancer-promoter interaction frequency following MENi (250 nM, 24 h) in SEM cells. For each gene with multiple MCC peaks, the most statistically significant promoter interaction is presented. (D) Genes with a significantly decreased enhancer-promoter contact and decreased expression after 24 h MENi (250 nM).

Figure 4

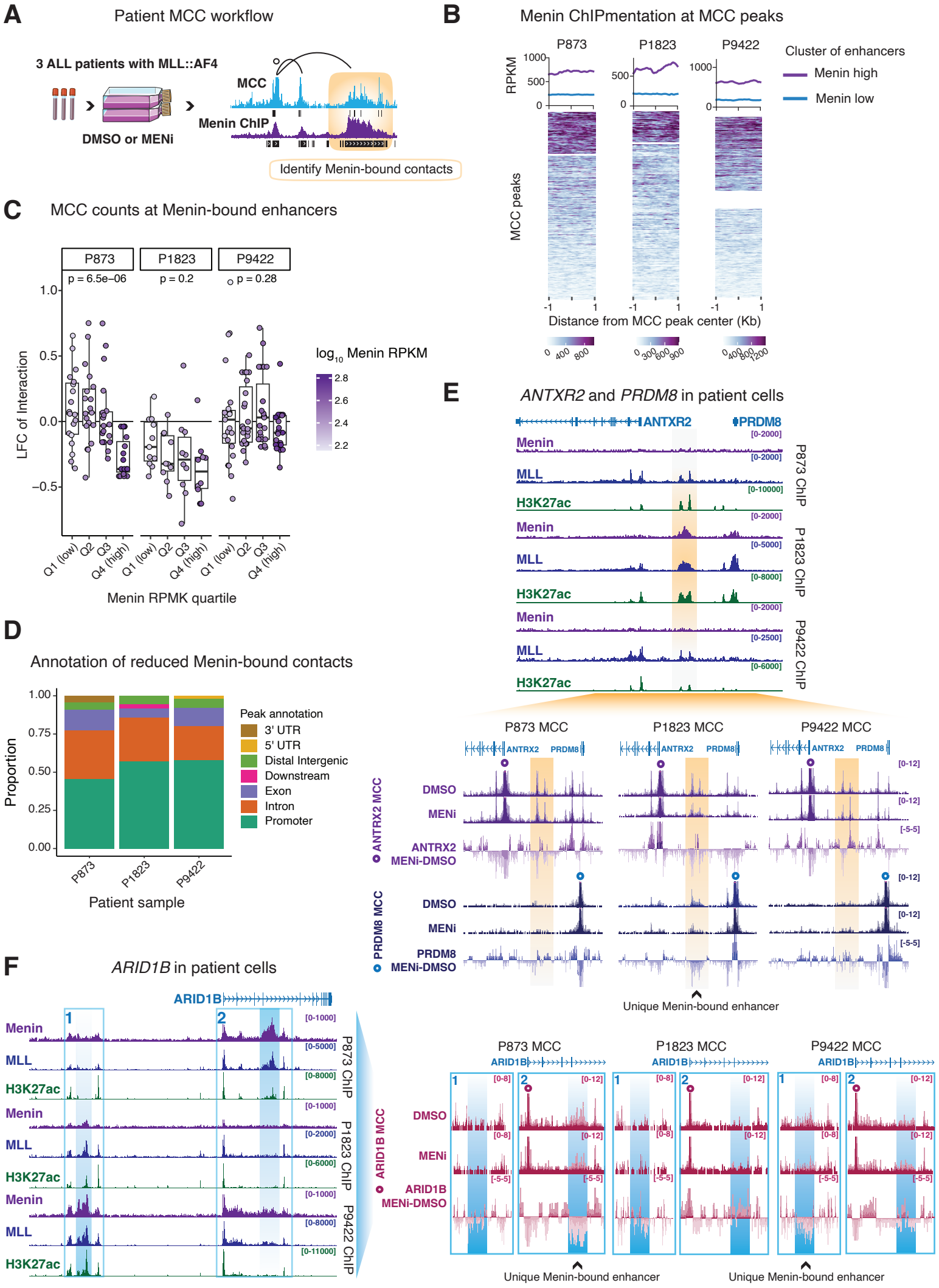
A
Patient MCC workflow
3 ALL patients with MLL::AF4
DMSO or MENi
MCC
Menin ChIP
Identify Menin-bound contacts
B
Menin ChIPmentation at MCC peaks
P873
P1823
P9422
RPKM
MCC peaks
Cluster of enhancers
Menin high
Menin low
Distance from MCC peak center (Kb)
C
MCC counts at Menin-bound enhancers
p = 6.5e−06
p = 0.2
p = 0.28
LFC of Interaction
log10 Menin RPKM
Q1 (low)
Q2
Q3
Q4 (high)
Menin RPMK quartile
D
Annotation of reduced Menin-bound contacts
Proportion
Peak annotation
3' UTR
5' UTR
Distal Intergenic
Downstream
Exon
Intron
Promoter
Patient sample
E
ANTXR2 and PRDM8 in patient cells
ANTXR2
PRDM8
Menin
MLL
H3K27ac
P873 ChIP
P1823 ChIP
P9422 ChIP
P873 MCC
P1823 MCC
P9422 MCC
ANTRX2 MCC
PRDM8 MCC
DMSO
MENi
ANTRX2 MENi-DMSO
PRDM8 MENi-DMSO
Unique Menin-bound enhancer
F
ARID1B ChIP
ARID1B
ARID1B MCC
ARID1B MENi-DMSO
Unique Menin-bound enhancer

Figure 4.: Menin-bound enhancers are sensitive to Menin inhibition in primary patient ALL cells. (A) Schematic of Micro-Capture-C experiment in primary patient cells. (B) Metaplots and associated heatmaps of Menin binding at MCC peaks in patient cells, clustered by Menin binding (hclust = 2). (C) Log2 fold changes in MCC at Menin-bound enhancers stratified into quartiles by Menin signal for each patient sample. *p*-values are reported from Kruskal-Wallis tests. (E) Visualization of Menin, MLL/MLL::AF4 and H3K27ac ChIPmentation (top, mean signal) and MCC (bottom, mean+whiskers), at *ANTRX* and *PRDM8* in primary patient cells. Menin-bound sites unique to Patient 1823 are highlighted in yellow. (E) Visualization of Menin, MLL/MLL::AF4 and H3K27ac ChIPmentation (left, mean signal) and MCC (right, mean+whiskers) at *ARID1B* in primary patient cells. Menin-bound sites unique to Patient 873 and Patient 9422 are boxed in blue.

Figure 5

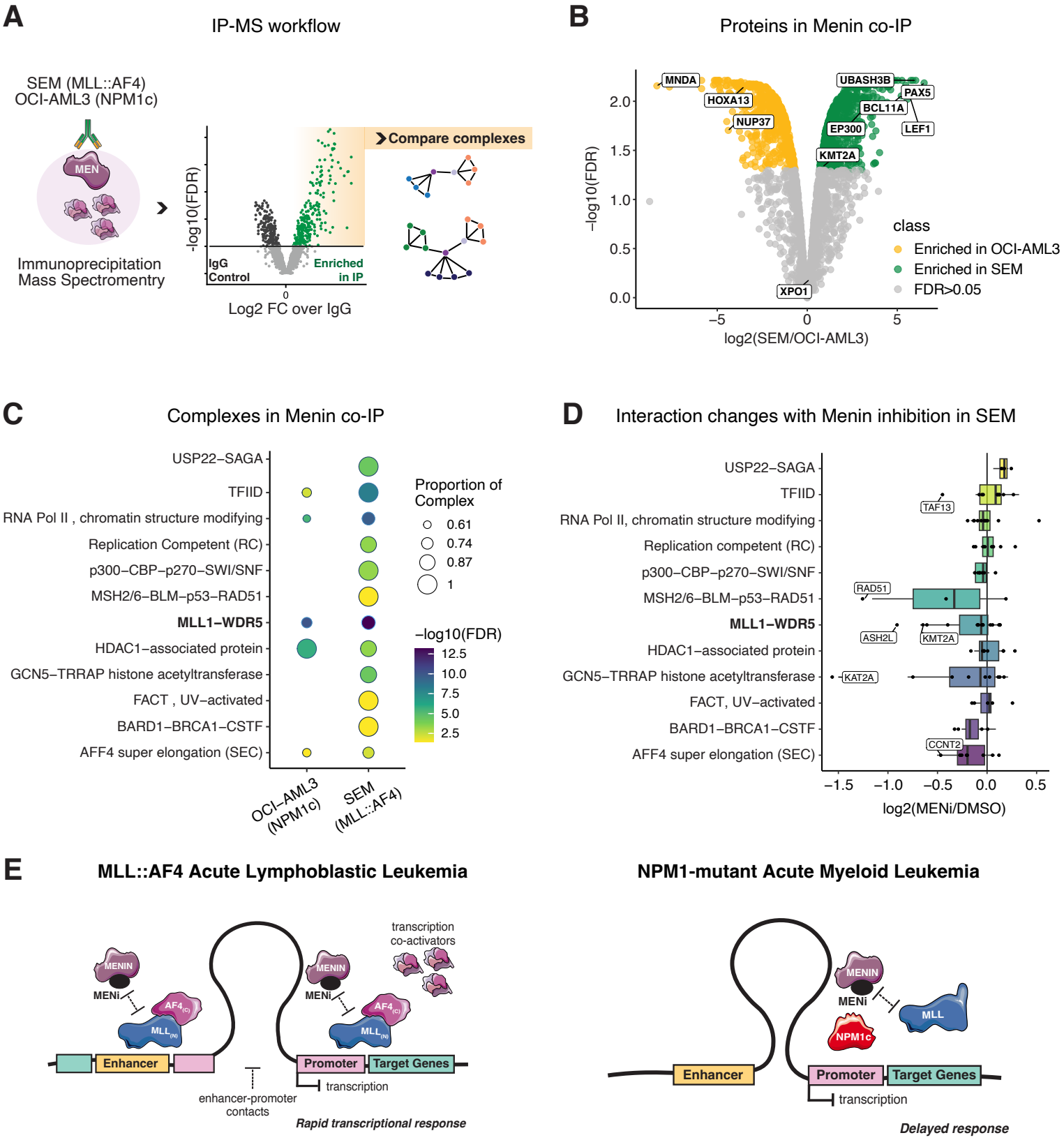
A
IP-MS workflow
SEM (MLL::AF4)
OCI-AML3 (NPM1c)
MEN
Immunoprecipitation
Mass Spectromentry
-log10(FDR)
IgG
Control
Enriched
in IP
0
Log2 FC over IgG
Compare complexes
B
Proteins in Menin co-IP
MNDA
HOXA13
NUP37
UBASH3B
PAX5
BCL11A
LEF1
EP300
KMT2A
XPO1
−log10(FDR)
2.0
1.5
1.0
0.5
0.0
−5
0
5
log2(SEM/OCI-AML3)
class
Enriched in OCI-AML3
Enriched in SEM
FDR>0.05
C
Complexes in Menin co-IP
USP22−SAGA
TFIID
RNA Pol II , chromatin structure modifying
Replication Competent (RC)
p300−CBP−p270−SWI/SNF
MSH2/6−BLM−p53−RAD51
MLL1−WDR5
HDAC1−associated protein
GCN5−TRRAP histone acetyltransferase
FACT , UV−activated
BARD1−BRCA1−CSTF
AFF4 super elongation (SEC)
OCI−AML3
(NPM1c)
SEM
(MLL::AF4)
Proportion of
Complex
0.61
0.74
0.87
1
−log10(FDR)
12.5
10.0
7.5
5.0
2.5
D
Interaction changes with Menin inhibition in SEM
USP22−SAGA
TFIID
RNA Pol II, chromatin structure modifying
Replication competent (RC)
p300−CBP−p270−SWI/SNF
MSH2/6−BLM−p53−RAD51
MLL1−WDR5
HDAC1−associated protein
GCN5−TRRAP histone acetyltransferase
FACT, UV−activated
BARD1−BRCA1−CSTF
AFF4 super elongation (SEC)
TAF13
RAD51
ASH2L
KMT2A
KAT2A
CCNT2
−1.5
−1.0
−0.5
0.0
0.5
log2(MENi/DMSO)
E
MLL::AF4 Acute Lymphoblastic Leukemia
MENIN
MENi
AF4(C)
MLL(N)
transcription
co-activators
Enhancer
Promoter
Target Genes
transcription
enhancer-promoter
contacts
Rapid transcriptional response
NPM1-mutant Acute Myeloid Leukemia
MENIN
MENi
MLL
NPM1c
Enhancer
Promoter
Target Genes
transcription
Delayed response

Figure 5.: Menin associates with transcriptional regulators in leukemia cells. (A) Schematic of IP-MS workflow. (B) Volcano plot comparing statistically enriched Menin interactors in SEM and OCI-AML3 cells. Proteins were pre-filtered on enrichment over IgG controls (FDR < 0.01) in each cell line. (C) Global enrichment (FDR < 0.05) of select complexes involved in transcription in Menin co-immunoprecipitations. (D) Log2 fold changes in protein abundance in Menin co-IPs from DMSO or MENi-treated (24 h 250nm) SEM cells. (E) Model of Menin activity in MLL::AF4 and NPM1-mutant leukemia: Menin associates more strongly with transcription co-activators and stabilizes enhancer-promoter proximity to activate genes in MLL::AF4 but not NPM1c AML.

Supplementary Figure 1

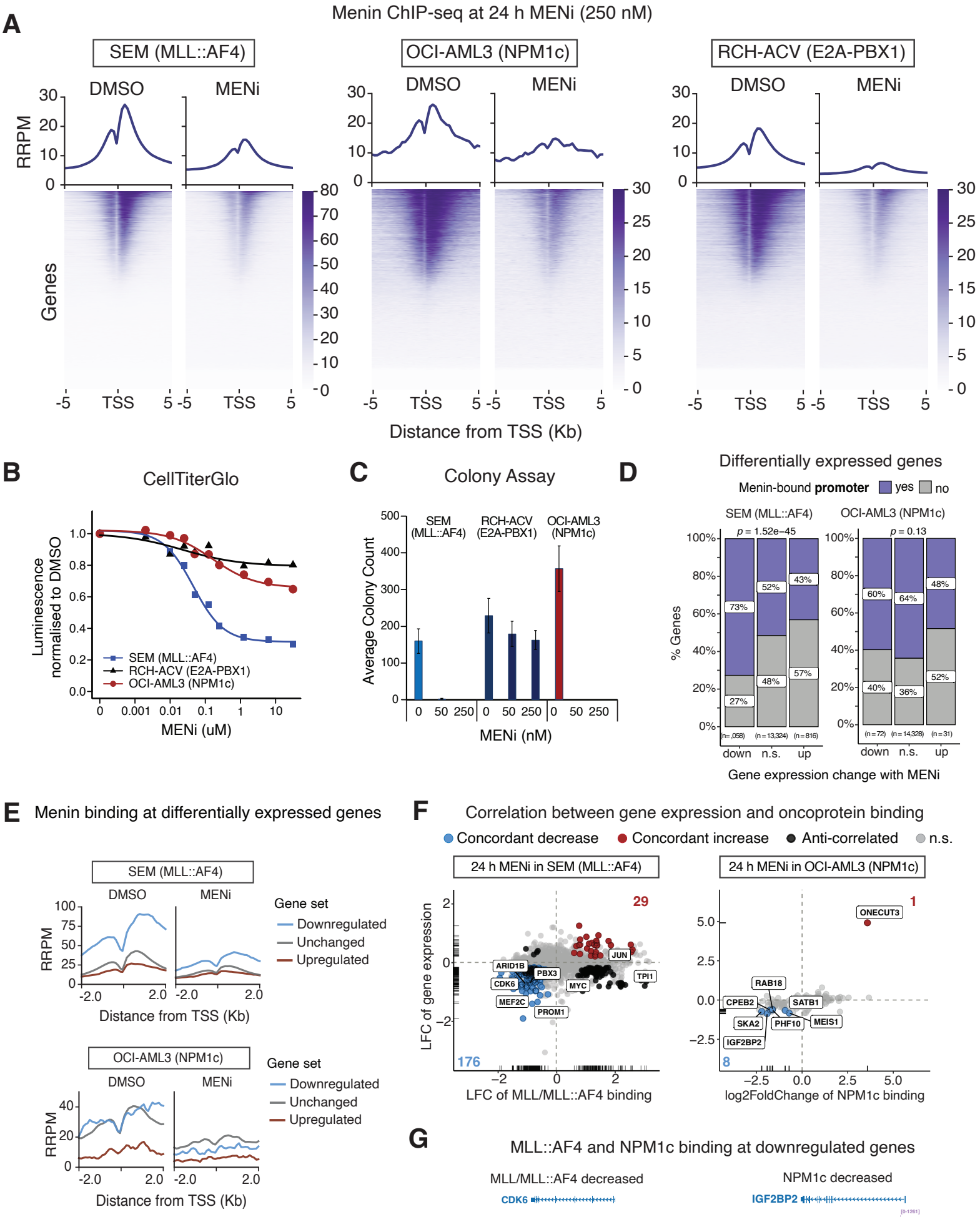

Supplementary Figure 1.: Association between Menin binding, cell viability, and transcription changes. (A) Menin ChIP-seq after 24 h treatment with DMSO or 250 nM Menin inhibitor VTP50469 (MENi) in SEM, OCI-AML3, and RCH-ACV cells. Metaplots show mean reference normalized reads per million (RRPM) centered on transcription start sites (TSS) genome-wide. (B) Dose response curves to MENi recorded at 48 h using CellTiterGlo (n = 5 for SEM and RCH-ACV cells, n = 3 for OCI-AML3 cells). (C) Colony forming units recorded after culture in Menin inhibitor (n=5). Error bars represent standard error. (D) Proportion of differentially expressed genes (n.s. = not significant) following MENi with Menin binding at the promoter (± 2 kb around the TSS). Reported *p*-values are from a Pearson chi-square test. (E) Mean Menin binding (RRPM = reference normalised ChIP-seq reads per million) in SEM and OCI-AML3 cells at promoters of differentially expressed genes in DMSO or MENi-treated cells. (F) Scatter plots correlating changes in gene expression and changes in MLL/MLL::AF4 or NPM1c binding following 24 h MENi (250nM). Genes are colored if they display a significant alteration (p-adj < 0.05) in both expression and MLL::AF4/NPM1c binding. (G) Examples of altered Menin, MLL/MLL::AF4, and NPM1c binding following 24 h MENi (250nM) in SEM cells (left) and OCI-AML3 cells (right).

Supplementary Figure 2

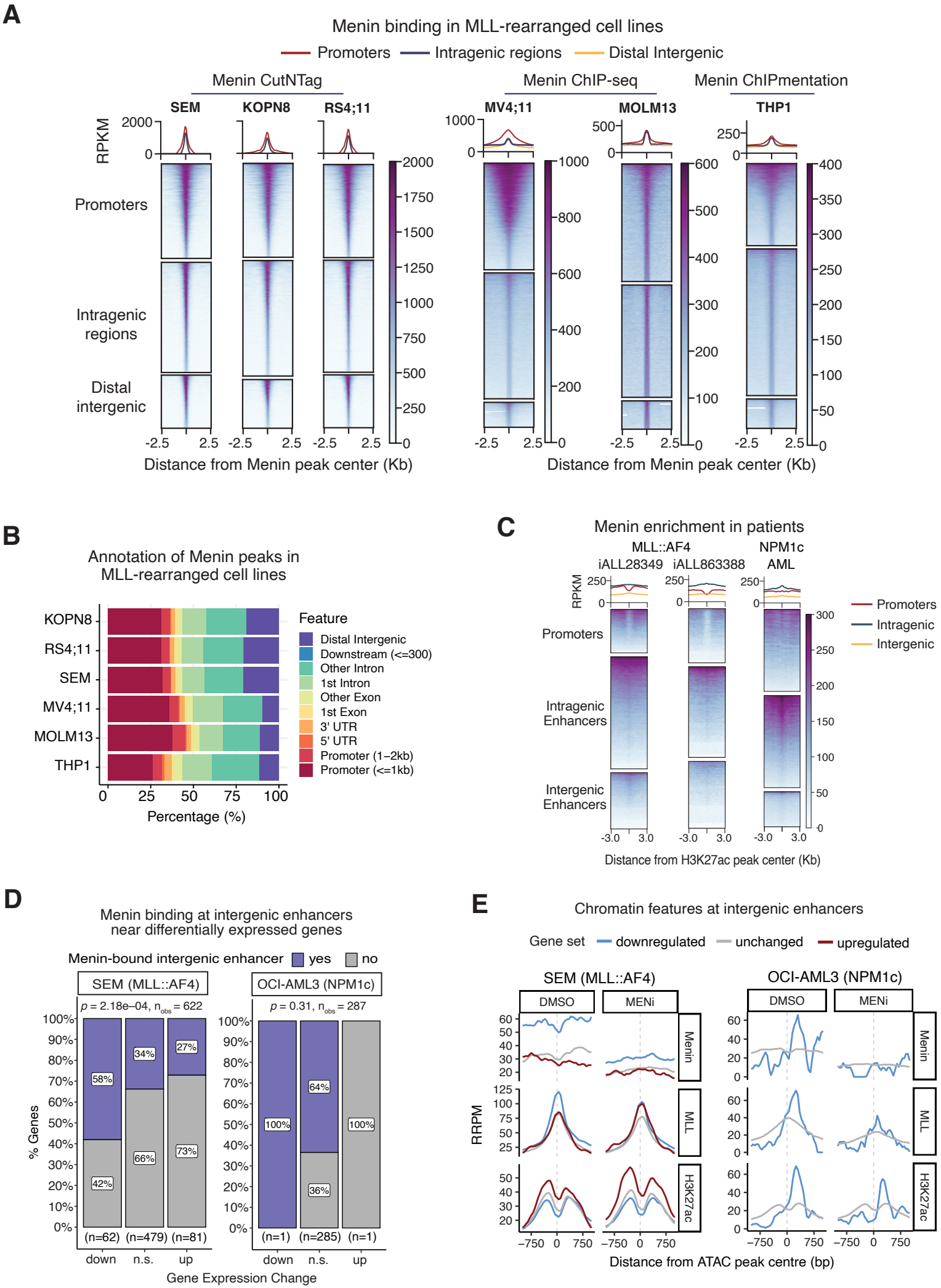

Supplementary Figure 2.: Menin binds enhancer elements. (A) Heatmaps and metaplots of mean Menin signal at promoters (±2 kb of a TSS), intragenic regions, and distal intergenic regions in cell lines with *MLL* translocations. (B) Annotation of Menin peaks in cell lines with *MLL* translocations. (C) Heatmaps of Menin ChIPmentation at promoters and enhancers, centred on H3K27ac peaks, in primary samples from two infant MLL::AF4 ALL patients (iALL28349, iALL863388) and one adult NPM1-mutated AML patient. (D) Association between Menin binding at intergenic enhancers and gene expression following 24 h of MENi (250 nM). *p*-values are reported from a Pearson chi-squared test. (E) Metaplots representing mean Menin, MLL, and H3K27ac signal at intergenic enhancers annotated to differentially expressed genes after 24 h of MENi (250 nM) in SEM and OCI-AML3 cells.

Supplementary Figure 3

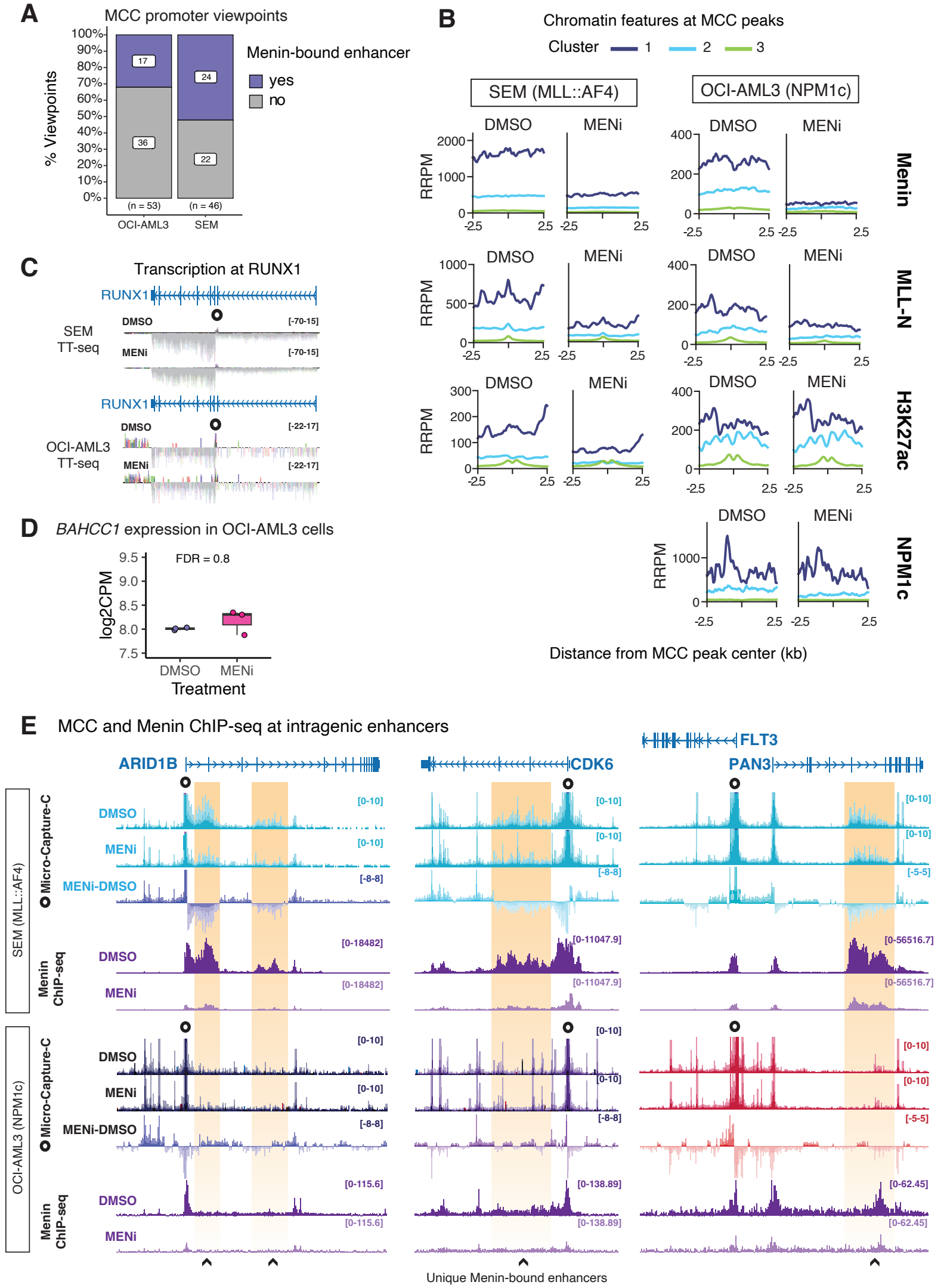

Supplementary Figure 3.: Micro-Capture-C reveals Menin-sensitive enhancers in SEM cells. (A) Proportion of genes selected for Micro-Capture-C promoter viewpoints annotated with whether they have a proximal Menin-bound enhancer, assigned by nearest TSS. (B) Mean Menin, MLL/MLL::AF4, H3K27ac, and NPM1c signal at MCC peaks in SEM cells and OCI-AML3 cells, clustered with k-means = 3 across all ChIP-seq samples per cell line. (C) *BAHCC1* expression after DMSO or 24 h MENi (250 nM) in OCI-AML3 cells, TT-seq data (CPM = counts per million). (D) Visualization of MCC (mean with whiskers) and Menin ChIP-seq (mean) data at *ARID1B*, *CDK6* and *FLT3*/*PAN3* in SEM and OCI-AML3 cells after 24 h MENi (250 nM). The capture viewpoint is shown as a circle at the gene promoters. Menin-bound enhancers in SEM cells are highlighted in yellow.

Supplementary Figure 4

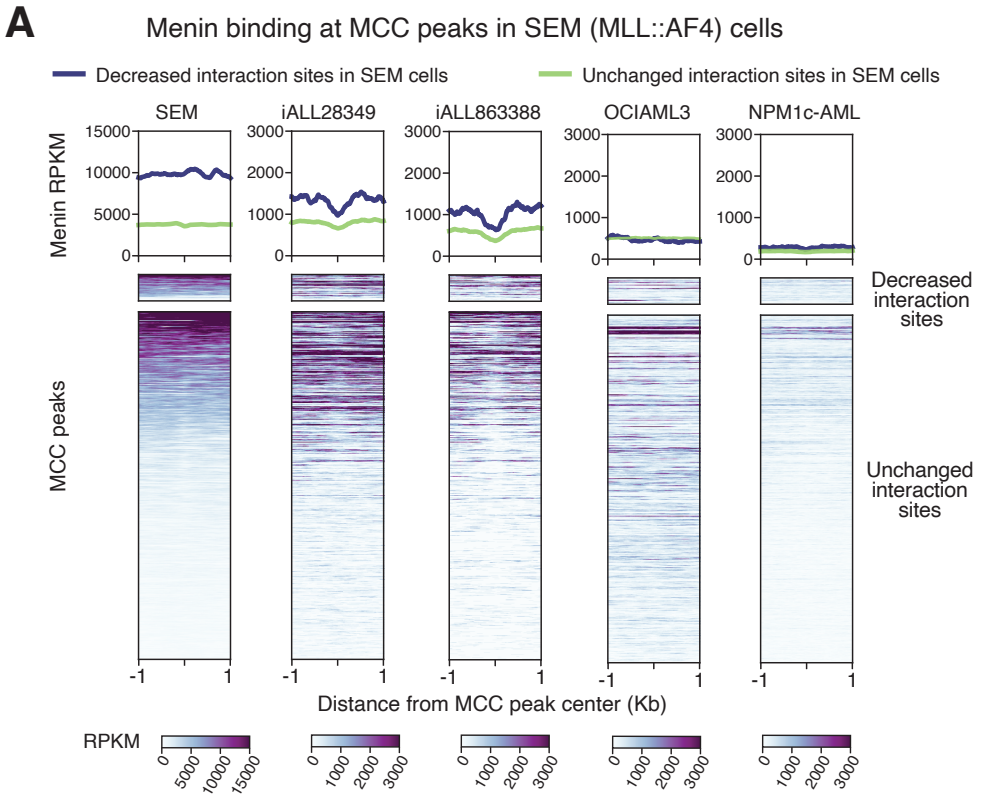

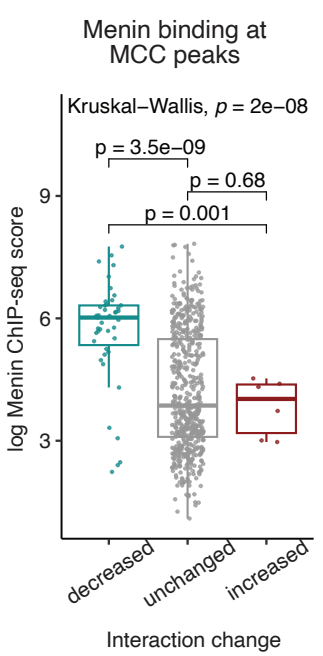

Supplementary Figure 4.: Menin-sensitive enhancers in SEM cells have high levels of Menin binding in SEM and patient samples. (A) Menin binding in cell lines (ChIP-seq in SEM and OCI-AML3 cells) and in primary patient cells (ChIPmentation in iALL28349, iALL863388, and NPM1c-AML) at MCC peaks in SEM cells. Menin signal at MCC peaks with a statistically significant (Mann Whitney U FDR q-value < 0.05, log2 fold change < 0) decrease in unique ligation junctions in SEM cells following MENi (250 nM, 24 h) is shown in dark blue on the metaplots and in the top cluster on the heatmaps. (B) Quantification of Menin ChIP-seq signal at differential MCC peaks in SEM cells.

Supplementary Figure 5

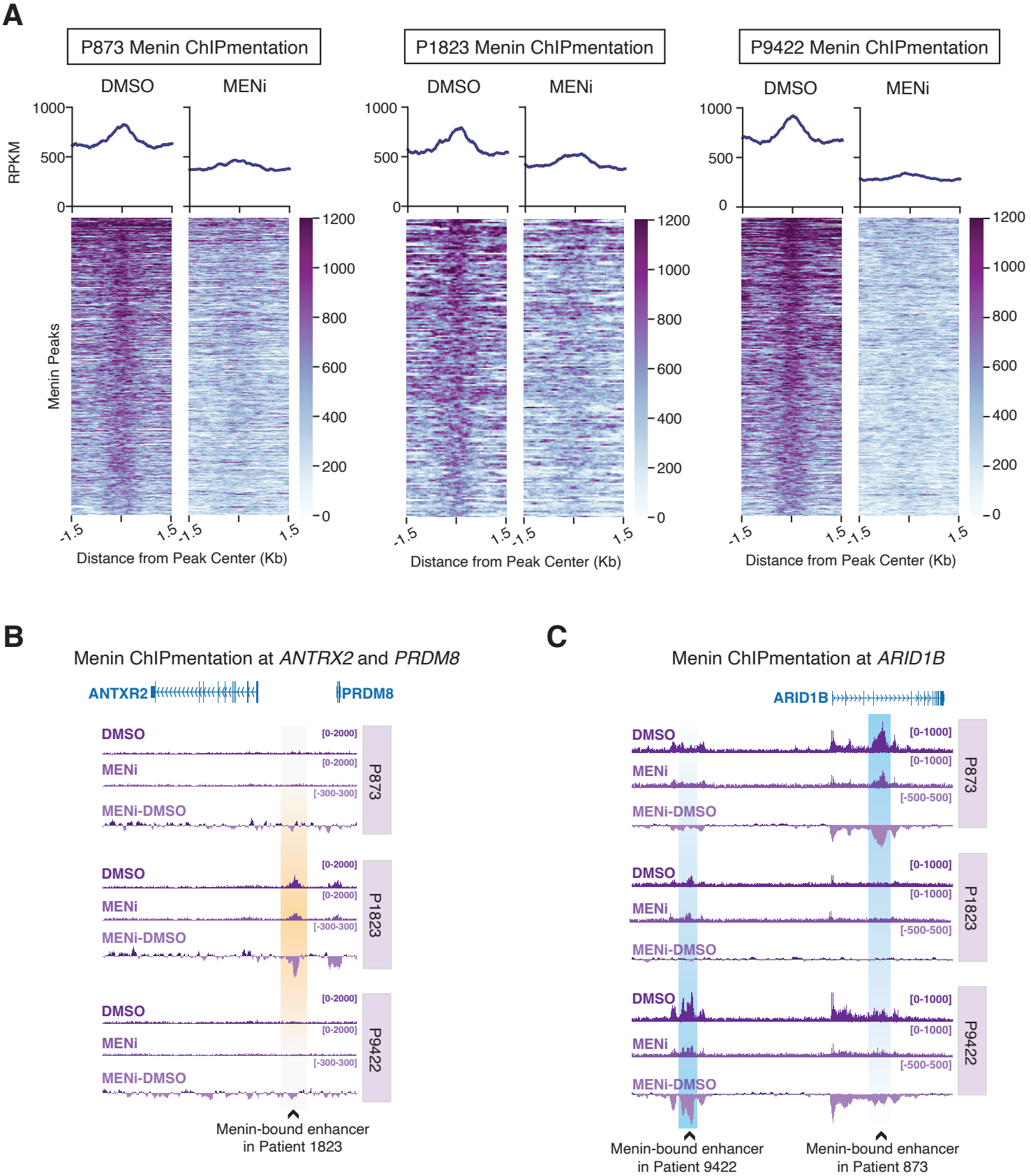

Supplementary Figure 5.: Menin is enriched at enhancers in MLL::AF4 primary patient samples. (A) Menin ChIPmentation at Menin peaks in primary patient cells treated with DMSO or 250 nM MENi for 24 h. (B) Menin ChIPmentation at *ANTRX2* and *PRDM8* in patient cells. (C) Menin ChIPmentation at *ARID1B* in patient cells.

Supplementary Figure 6

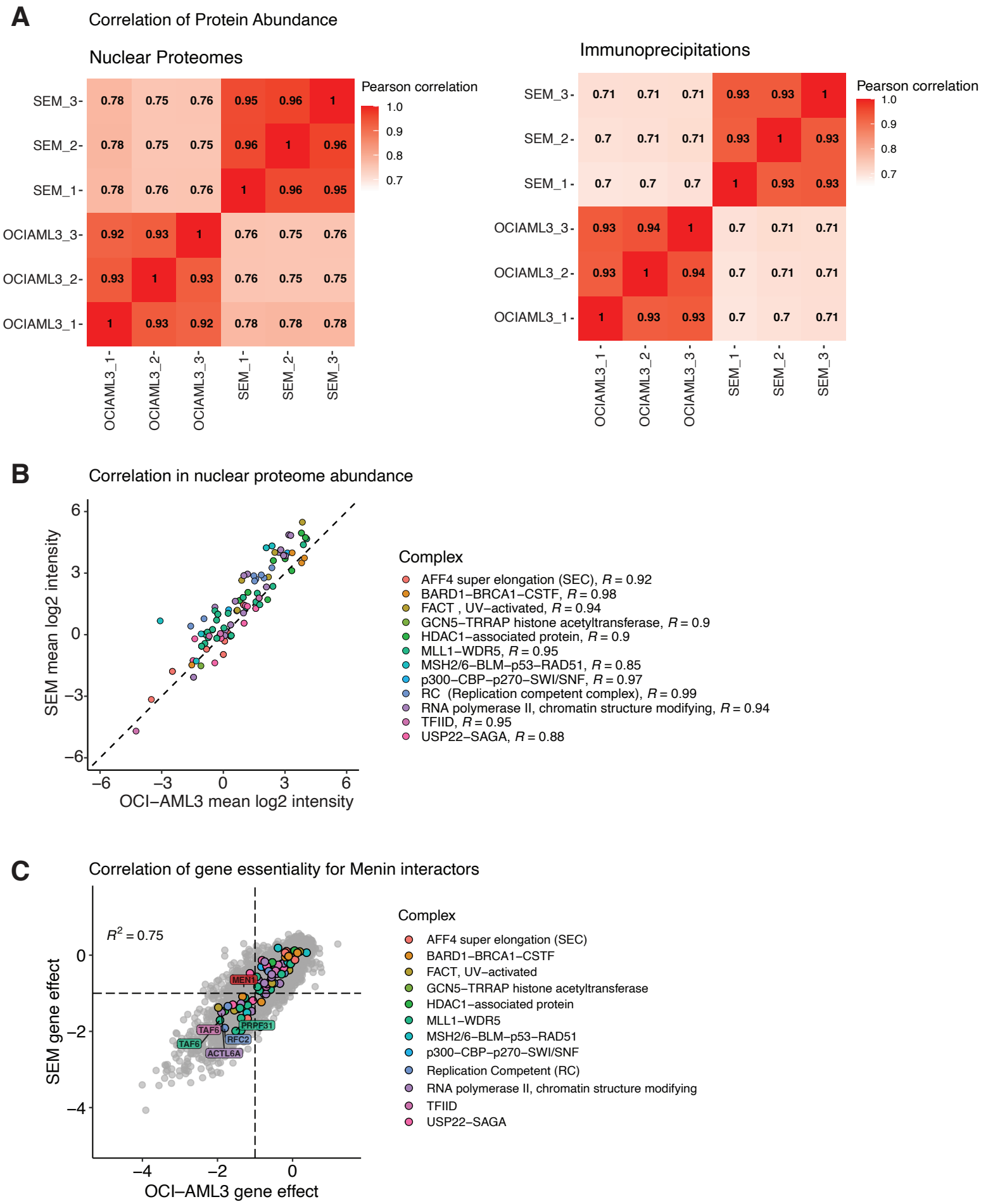

Supplementary Figure 6:. Menin co-IPs have different enrichments of transcription activators despite highly correlated interactomes and nuclear proteomes between cell lines. (A) Pearson correlations between nuclear proteome samples computed on log2-transofrmed and imputed intensities. (B) Correlation in the abundance of differentially enriched complex components in the nuclear proteomes of SEM and OCI-AML3 cells. The grey dashed line represents a slope of 1. Pearson *R* values are shown for each complex. (C) Correlation between the gene effect scores reported in DepMap for SEM and OCI-AML3 CRISPR screens. Proteins within complexes specifically enriched in SEM cells are colored. Genes with an effect score of < -1 in both cell lines are labelled.

Supplementary Table 1: Antibodies for chromatin immunoprecipitation

Antibody	Reference	Application (per 1 × 10^7 cells)
Menin	Bethyl A300-105A	2 μg for ChIP, 1 μg for IP
MLL N-terminus	Bethyl A300-086A	2 μg
H3K27ac	Diagenode C15410196	1.25 μg
H3K4me1	Diagenode C15410194	3 μg
H3K4me3	Diagenode C15410003	2.6 μg
NPM1c	ThermoFisher PA1-46356	2 μg
Rabbit IgG	Cell Signalling DA1E	1 ug

Supplementary Table 2: Sources of publicly available sequencing data

Dataset	Reference
OCI-AML3 ATAC-seq	GSM5114291
SEM Menin AutoCUTnTag	GSM5139719
KOPN8 Menin AutoCUTnTag	GSM5139645
RS4;11 Menin AutoCUTnTag	GSM5139689
iALL_28349 Menin ChIPmentation	GSM8657204
iALL_28349 H3K27ac ChIPmentation	GSM8657208
iALL_863388 Menin ChIPMentation	GSM8657184
iALL_863388 H3K27ac ChIPMentation	GSM8657191
MV4;11 Menin ChIP-seq	GSM5858383
MOLM13 Menin ChIP-seq	GSM3635683